Electronic Supplementary Material (ESI) for ChemComm.

Supplementary Information

A Cu(II)-MOF Capable of Fixing CO_2 From Air and Showing High Capacity H_2 and CO_2 Adsorption

Vivekanand Sharma,[‡a] Dinesh De,[‡a] Ranajit Saha,[b] Ranjita Das,[b] Pratim Kumar Chattaraj,*[b] and Parimal K. Bharadwaj*[a]

[a]Department of Chemistry, Indian Institute of Technology Kanpur, Kanpur 208016, India

[b]Department of Chemistry, Indian Institute of Technology Kharagpur, Kharagpur 721302, India

Experimental Section

Materials. The metal salts and other reagent grade chemicals were purchased and used without further purification from commercial suppliers (Sigma-Aldrich, Alfa Aesar, TCI, and others). All the solvents were from S. D. Fine Chemicals, India. These solvents were purified following standard conventional methods prior to use.

Physical Measurements

The following Spectroscopic data were collected. IR spectra (KBr disk, 400−4000 cm^{-1}) were recorded on a Perkin-Elmer model 1320 spectrometer. Powder X-ray diffraction (PXRD) patterns were recorded with a Bruker D8 Advance diffractometer equipped with nickel-filtered Cu K_α (1.5418 Å) radiation. The tube voltage and current were 40 kV and 40 mA, respectively. Thermogravimetric analyses (TGA) (heating rate of 5 °C/min under nitrogen atmosphere) were performed with a Mettler Toledo Star System. ^{1}H NMR and ^{13}C NMR spectra were recorded either on a JEOL ECX 500 FT (500, 125 MHz respectively) or on a JEOL ECS 400 FT (400, 100 MHz respectively) instrument in $CDCl_3$ or in DMSO-d_6 with Me_4Si as the internal standard. The ESI-Mass data were obtained in a WATERS-Q-Tof Premier Mass Spectrometer. Melting points were recorded on an electrical melting point apparatus from PERFIT India and were uncorrected.

Synthesis of the linker, H_4L

Synthesis of the ligand 5′-amino-1,1′:4′,1″-terphenyl-3,3″,5,5″-tetracarboxylic acid (**H_4L**; Scheme S1) was achieved in several steps following literature procedure.[1]

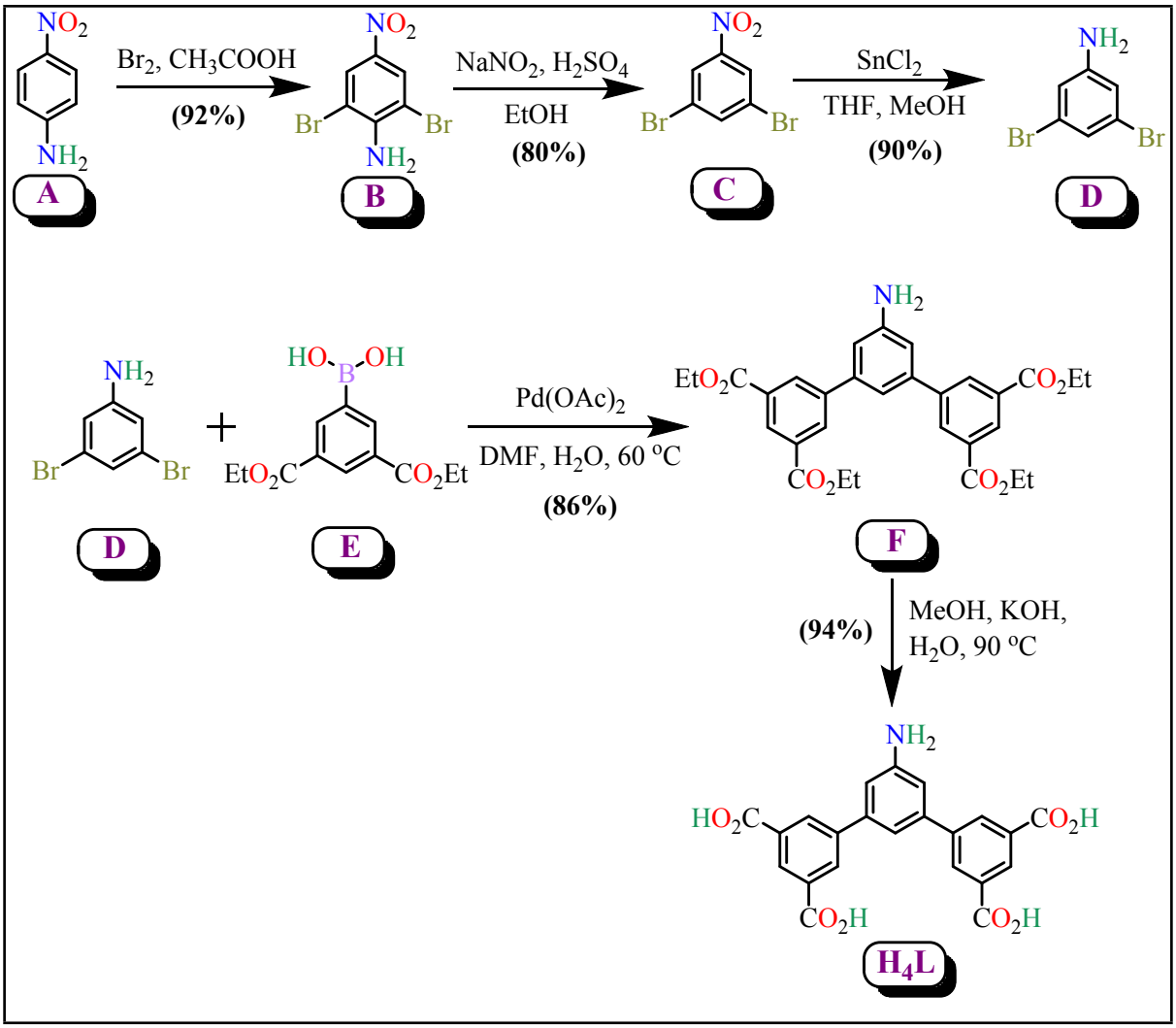

Scheme S1. Synthetic route for ligand **H_4L.**

Synthesis of 2,6-dibromo-4-nitroaniline (B)

A solution of *p*-nitroaniline (5.00 g, 36.20 mmol) in glacial acetic acid (45 mL) was vigorously stirred during the addition of bromine (4 mL, 78 mmol) in glacial acetic acid (28 mL) at 65 °C for about 4 h. A very heavy precipitate formed after about 30% of the bromine had been added and the precipitate was re-dissolved by the addition of hot water (8 mL), and then the remaining bromine solution was added. After complete addition, the reaction continued for overnight. Then

the mixture was poured into slurry of water and ice. The precipitate was filtered and washed thoroughly with water and the dried in air. The reaction afforded 9.85 g (92% yield) of the title compound as a yellow-green solid. ^{1}H NMR (400 MHz, $CDCl_3$): δ = 8.33 (s, 2H), 5.28 (br s, 2 H) ppm.

Synthesis of 3,5-dibromonitrobenzene (C).

To a stirred mixture of 2,6-dibromo-4-nitroaniline (5.00g, 16.90 mmol), ethanol (55 mL) and concentrated sulfuric acid (6 mL) at 80°C, sodium nitrite (3.60 g, 52 mmol) was added in portions as rapidly as effervescence would permit. The reaction mixture was allowed to stir at 80 °C for 40 h. Then the mixture was allowed to cool, poured into ice water and the solids were collected by filtration and washed with water. The 3,5-dibromonitrobenzene was recrystallized by dissolving in boiling ethanol and filtering the hot solution. On cooling, the reaction afforded 3.78 g (80% yield) with orange coloured crystals. ^{1}H NMR (500 MHz, $CDCl_3$): δ = 8.32 (d, J=1.7 Hz, 2 H), 7.99 (t, J=1.7 Hz, 1 H) ppm.

Synthesis of 3,5-dibromoaniline(D).

To a solution of 3,5-dibromonitrobenzene (1.21 g, 39.87 mmol) in methanol (15 mL) and THF (5 mL) stirred under air, tin(II) chloride dihydrate (4.80 g, 21.27 mmol) was added in portions slowly. The mixture was allowed to stir at about 60 °C temperature for 20 h. The solvent was then evaporated *in vacuo*, and an aqueous solution of sodium hydroxide (4.16 gm in 50 ml water) was added. The stirring was continued for 2 h. Finally, the reaction mixture was extracted with chloroform in water. The combined organic layer was dried over Na_2SO_4, and the solvent was removed *in vacuo*. The reaction afforded 0.98 g (90% yield) of the desired compound as a brown solid. ^{1}H NMR (400 MHz, $CDCl_3$): δ = 7.00 (t, J=1.5 Hz, 1 H), 6.73 (d, J= 1.5 Hz, 2 H), 3.75 (br s, 2 H) ppm.

Synthesis of 3′-amino-1,1′:4′,1″-terphenyl-3,3″,5,5″-tetracarboxylate (F).

A solution of 3,5-bis(ethoxycarbonyl)phenylboronic acid (2.80 g, 10.52 mmol), and 3,5-dibromoaniline (1.00 g, 3.98 mmol) in DMF (10 mL) was mixed with a solution of sodium carbonate (1.68 g, 15.85 mmol) and palladium acetate (40 mg) in water (15 mL). The mixture was allowed to stirr at 60°C for overnight in nitrogen atmosphere. The mixture was allowed to cool at room temperature and then water (150 mL) was added to it. The compound was extracted with ethyl acetate in water. The extracted ethyl acetate with the compound was passed through anhydrous sodium sulfate and evaporated *in vacuo*. After that it was purified by column chromatography using silica gel (200 mesh) with 40 % ethyl acetate in *n*-hexane. The experiment affords 3′-amino-1,1′:4′,1″-terphenyl-3,3″,5,5″-tetracarboxylate (yield: 4.8 g, 86% based on 3,5-dibromoaniline) as brown colored amorphous compound. ^{1}H NMR (400 MHz, $CDCl_3$): δ = 8.64 (s, 2H), 8.42 (d, 4H), 7.29 (s, 1H), 7.08 (s, 2H), 4.42 (q, 8H), 1.42 (t, 12H) ppm; ^{13}C (100 MHz, $CDCl_3$): δ = 165.87, 141.66, 141.47, 132.35, 131.56, 129.65, 117.41, 114.55, 61.58, 14.44 ppm.

Synthesis of 3′-amino-1,1′:4′,1″-terphenyl-3,3″,5,5″-tetracarboxylic acid (H_4L).

To a solution of ester **F** (2.00 g, 3.75 mmol) in methanol (100 mL) and water (50 mL), KOH (1.46 g, 26.07 mmol) was added in heating condition at 80 °C. The mixture was refluxed overnight. After removal of most of the solvent *in vacuo*, water was added to fully dissolve the precipitate and acidified with concentrated HCl upto pH~3 in ice bath. The yellow precipitate formed was collected by filtration, washed with ice cold water and dried in vacuum to obtain the ligand **H_4L** with an yield of 1.48 g (94%). m.p.>300°C; ^{1}H NMR (400 MHz, DMSO-d_6): δ = 8.42 (t, 2H), 8.36 (d, 4H), 7.12 (s, 1H), 6.98 (d, 2H) ppm; ^{13}C NMR (100 MHz, DMSO-d_6): δ = 167.10, 150.80, 142.01, 140.55, 132.49, 131.74, 129.32, 113.22, 112.66; ESI-MS: (m/z): 420

(100%) [M-H]. Anal. calcd. for $C_{22}H_{15}NO_8$: C, 62.71; H, 3.59; N, 3.32%. Found: C, 62.94; H, 3.71; N, 3.37%.

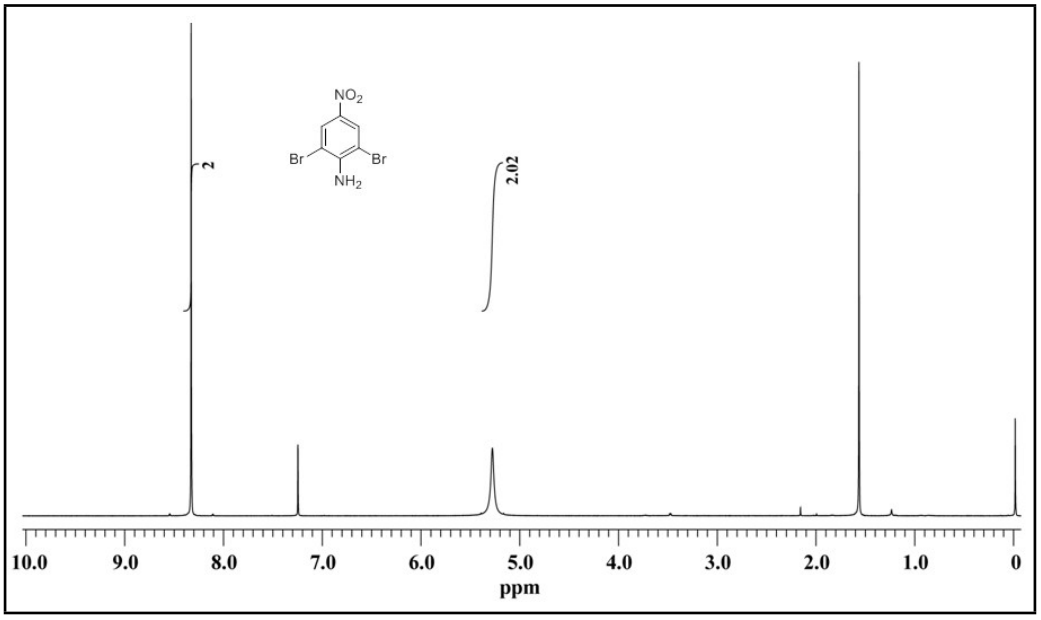

Fig. S1 The ^{1}H NMR spectrum of **B**.

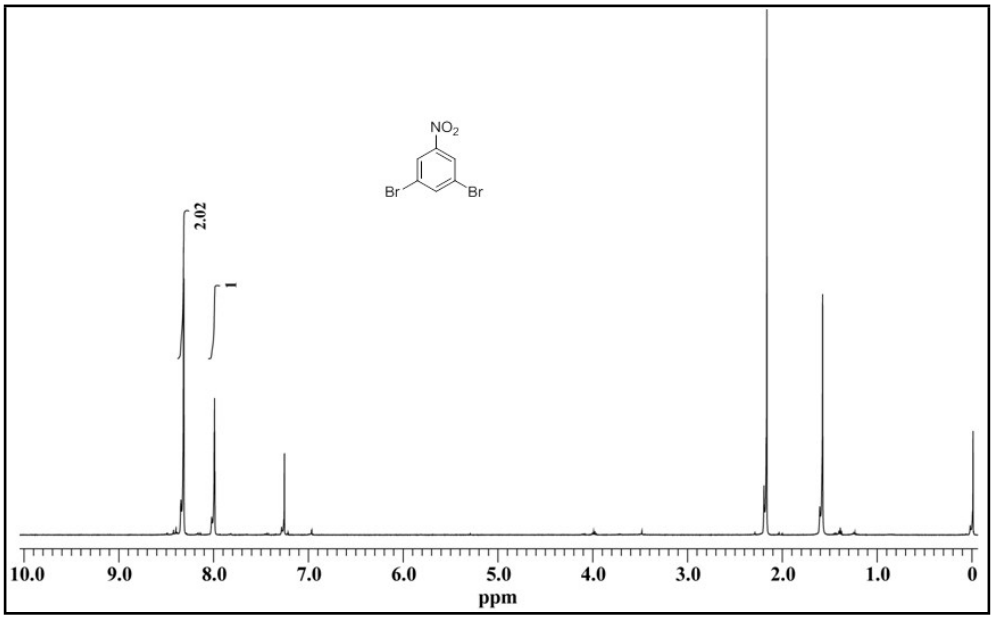

Fig. S2 The ^{1}H NMR spectrum of **C**.

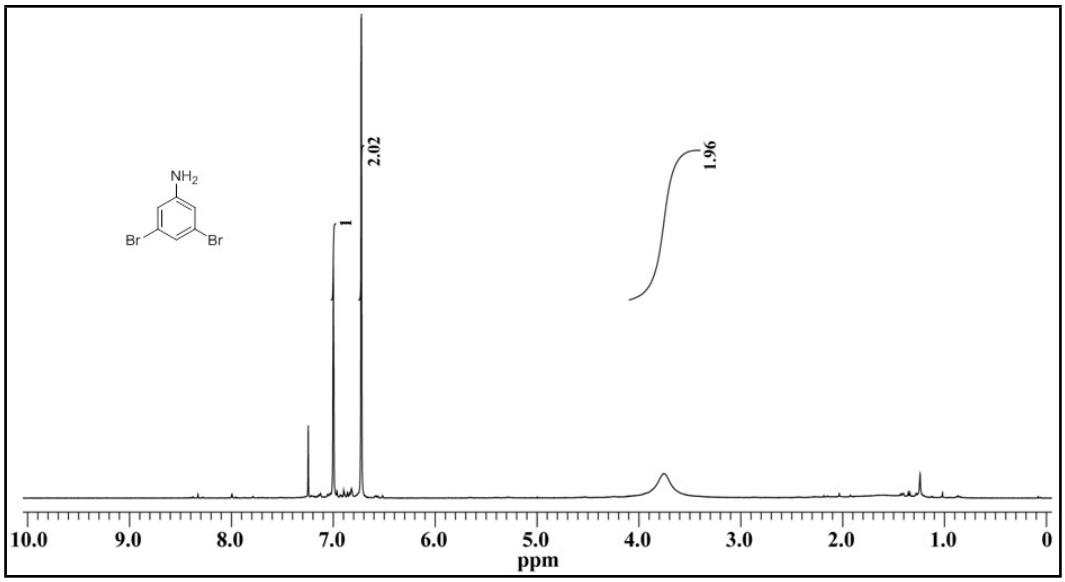

Fig. S3 The ^{1}H NMR spectrum of **D**.

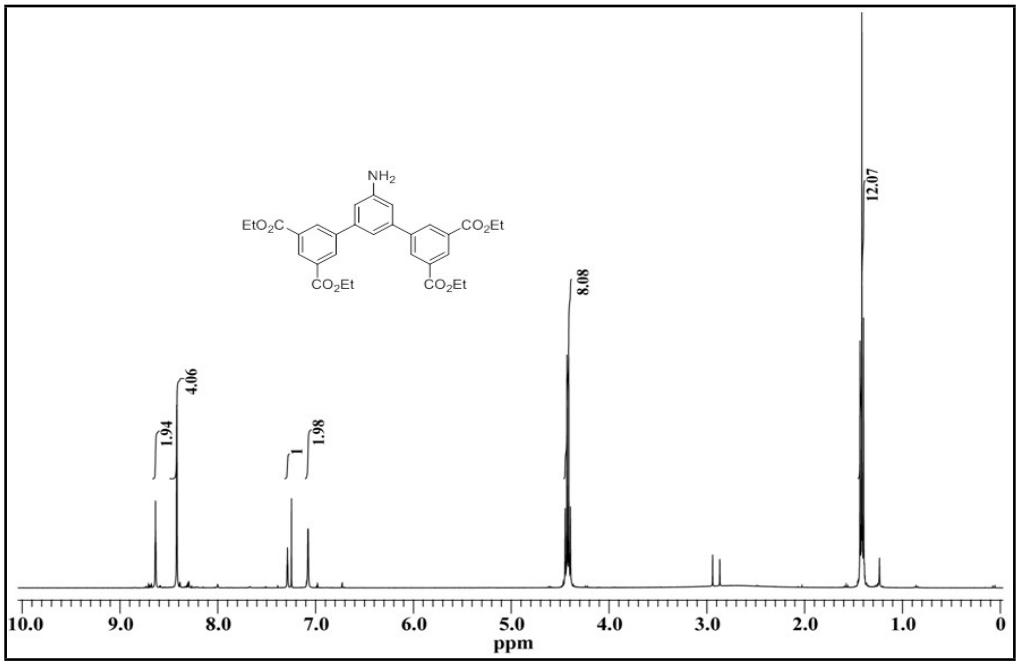

Fig. S4 The ^{1}H NMR spectrum of **F**.

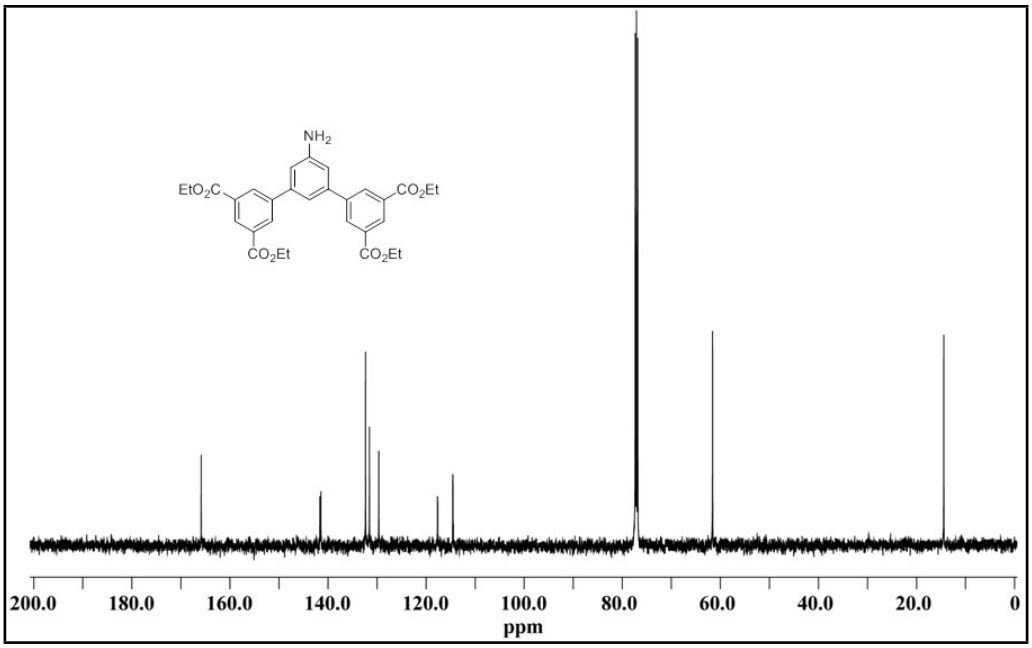

Fig. S5 The ^{13}C NMR spectrum of **F**.

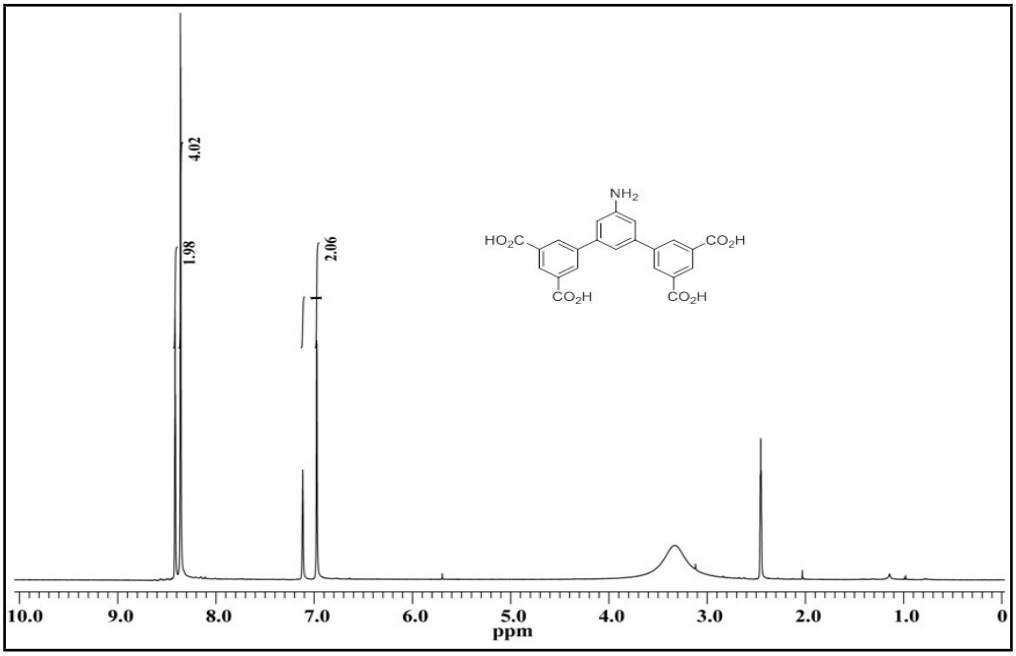

Fig. S6 The ^{1}H NMR spectrum of **H_4L**.

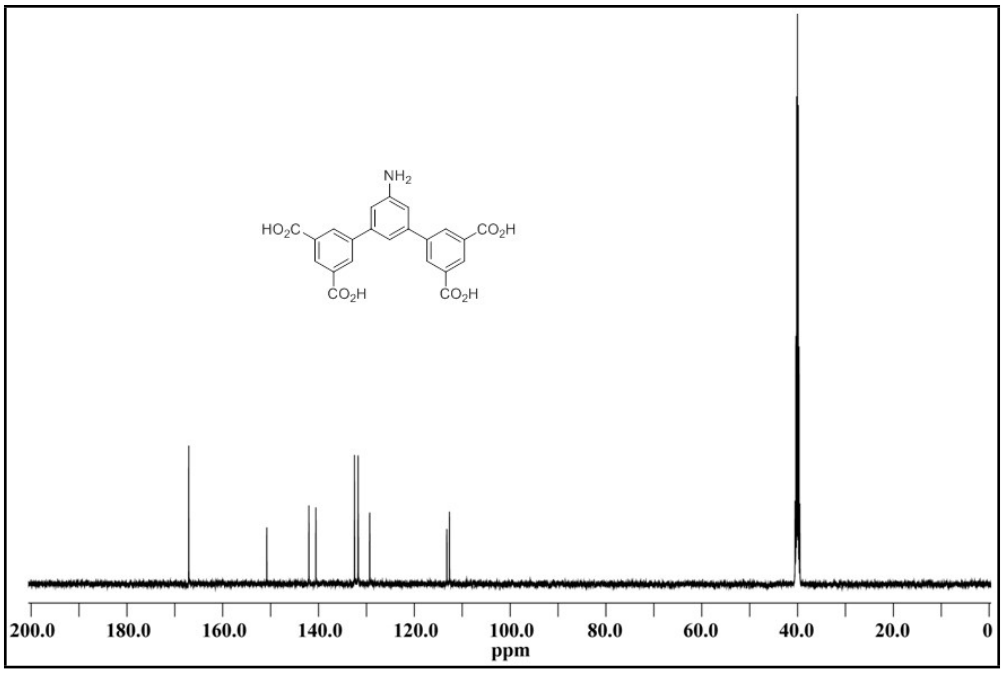

Fig. S7 The ^{13}C NMR spectrum of $\mathbf{H_4L}$.

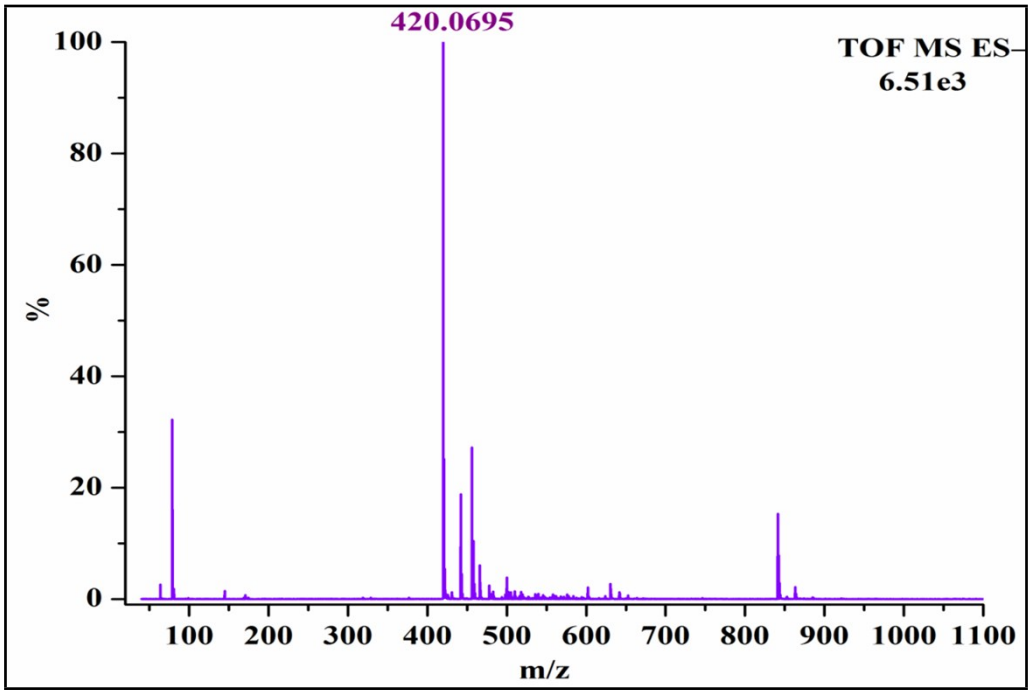

Fig. S8 ESI-MS spectrum (negative mode) of $\mathbf{H_4L}$.

Synthesis of $\{[Cu_6(L)_3(H_2O)_6]\cdot(14DMF)(9H_2O)\}_n$ (1). $Cu(NO_3)_2\cdot 3H_2O$ (25 mg, 0.104 mmol), and **H_4L** (20 mg, 0.048 mmol) were dissolved in 2mL DMF, 1 mL H_2O, and one drop conc. HCl. The mixture was placed in a Teflon-lined stainless steel autoclave and heated under autogenous pressure to 90 °C for 3 days and then allowed to cool to room temperature. Blue colored needle shaped crystals of **1** were collected by filtration and washed with DMF. Finally the crystal was dried in the air. Yield ~57%. FTIR (KBr pellets): 3422.63 cm^{-1} (broad), 2929.66 cm^{-1} (m), 1662.96 cm^{-1} (m), 1587.17 cm^{-1} (s), 1367.69 cm^{-1} (m), 1098.30 cm^{-1} (s), 776.63 cm^{-1} (s), 730.99 cm^{-1} (s). Anal. Calcd. For $C_{108}H_{161}N_{17}O_{53}Cu_6$: C, 44.32; H, 5.54; N, 8.14%. Found: C, 44.67; H, 5.71; N, 8.21%.

General Procedure for the Coupling of Epoxides with CO_2. Epoxide (20 mmol), catalyst **1′** (0.2 mol % per copper paddlewheel unit) and co-catalyst Bu_4NBr (1 mmol) were taken in a schlenk tube. The reaction mixture was then stirred at room temperature under CO_2 (99.999%) bubbling. When the reaction was completed, 5 mL CH_2Cl_2 was added and the mixture was filtered to separate the catalyst. All cyclic carbonates were isolated by column chromatography and analyzed through ^1H NMR spectroscopy.

In a similar way, the conversion of atmospheric CO_2 into cyclic carbonate was carried out. Instead of using CO_2 from direct source, we have purged the laboratory air as CO_2 source and the mixture was allowed to stir for 24 h.

X-Ray Structural Studies

The crystal data for **1** has been collected on a Bruker SMART CCD diffractometer (Mo Kα radiation, λ = 0.71073 Å). The program SMART[2] was used for collecting frames of data,

indexing reflections, and determining lattice parameters, SAINT[2] for integration of the intensity of reflections and scaling, SADABS[3] for absorption correction, and SHELXTL[4] for space group and structure determination and least-squares refinements on F^2. The crystal structure were solved and refined by full-matrix least-squares methods against F2 by using the program SHELXL-2014[5] using Olex-2 software.[6] All the non-hydrogen atoms were refined with anisotropic displacement parameters. Hydrogen positions were fixed at calculated positions and refined isotropically. The lattice solvent molecules of **1** could not be modeled satisfactorily due to the presence of severe disorder. Therefore, PLATON/SQUEEZE[7] program has been performed to discard those disordered solvents molecules. Crystallographic data has been deposited at the Cambridge Crystallographic Data Center and CCDC number: 1555358. Lattice parameters of the compound, data collection and refinement parameters are summarized in Table S1 and selected bond distances and bond angles are given in Table S2.

Table S1. Crystal and structure refinement data.

Parameters	**1**
Empirical formula	$C_{108}H_{161}N_{17}O_{53}Cu_6$
Formula wt.	2926.786
Temperature (K)	100(2)
Radiation Source	Mo K_α
Wavelength (Å)	0.71073
Crystal system	Orthorhombic
Space group	$Cmc2_1$
a, Å	24.8326(16)
b, Å	33.3574(16)
c, Å	18.3852(10)

α (°)	90
β (°)	90
γ (°)	90
V, Å^3	15229.4(15)
Z	4
ρ_{calc} (g/cm^3)	0.754
μ, mm^{-1}	0.864
F(000)	3456
Refl. Collected	94523
R_{int}	0.0846
Independent refl.	13399
Refinement method	Full-matrix least-squares on F^2
GOOF	1.007
Final R indices	R1 = 0.0575
[I>2σ(I)]	wR2 = 0.1392
R indices	R1 = 0.0949
(all data)	wR2 = 0.1529

Table 2. Selected bond distances (Å) and bond angles (°) of **1.**

Cu2 O6 1.977(4)	Cu2 O12 1.923(4)	Cu2 O8 1.974(4)	Cu2 O10 1.909(4)
Cu2 O2W 2.162(5)	Cu4 Cu3 2.6374(12)	Cu4 O4 2.021(4)	Cu4 O4 2.021(4)
Cu4 O1 1.950(4)	Cu4 O1 1.950(4)	Cu4 O4W 2.096(6)	Cu1 O11 1.938(4)
Cu1 O9 1.909(4)	Cu1 O7 2.001(4)	Cu1 O5 1.955(4)	Cu1 O1W 2.125(5)
Cu3 O3 1.986(5)	Cu3 O3 1.986(5)	Cu3 O2 1.853(5)	Cu3 O2 1.853(5)
Cu3 O3W 2.188(5)			

O6 Cu2 Cu1 85.14(12)	O6 Cu2 O2W 101.7(2)	O12 Cu2 Cu1 84.01(13)
O12 Cu2 O6 169.10(18)	O12 Cu2 O8 90.5(2)	O12 Cu2 O2W 89.2(2)
O8 Cu2 Cu1 83.20(14)	O8 Cu2 O6 87.1(2)	O8 Cu2 O2W 99.4(2)
O10 Cu2 Cu1 84.64(13)	O10 Cu2 O6 90.0(2)	O10 Cu2 O12 90.1(2)
O10 Cu2 O8 167.69(19)	O10 Cu2 O2W 92.9(2)	O2W Cu2 Cu1 172.76(19)

O4 Cu4 Cu3 84.11(11)	O4 Cu4 Cu3 84.11(11)	O4 Cu4 O4 87.6(3)
O4 Cu4 O4W 96.4(2)	O4 Cu4 O4W 96.4(2)	O1 Cu4 Cu3 82.49(12)
O1 Cu4 Cu3 82.50(12)	O1 Cu4 O4 166.17(17)	O1 Cu4 O4 166.18(17)
O1 Cu4 O4 87.67(18)	O1 Cu4 O4 87.67(18)	O1 Cu4 O1 94.0(3)
O1 Cu4 O4W 97.1(2)	O1 Cu4 O4W 97.1(2)	O4W Cu4 Cu3 179.3(3)
O11 Cu1 Cu2 84.23(12)	O11 Cu1 O7 90.86(19)	O11 Cu1 O5 167.23(18)
O11 Cu1 O1W 101.6(2)	O9 Cu1 Cu2 82.40(13)	O9 Cu1 O11 89.74(19)
O9 Cu1 O7 165.80(19)	O9 Cu1 O5 90.3(2)	O9 Cu1 O1W 99.5(2)
O7 Cu1 Cu2 83.55(13)	O7 Cu1 O1W 94.3(2)	O5 Cu1 Cu2 83.12(13)
O5 Cu1 O7 86.0(2)	O5 Cu1 O1W 91.0(2)	O1W Cu1 Cu2 173.9(2)
O3 Cu3 Cu4 82.50(14)	O3 Cu3 Cu4 82.50(14)	O3 Cu3 O3 83.9(4)
O3 Cu3 O3W 94.25(18)	O3 Cu3 O3W 94.25(18)	O2 Cu3 Cu4 85.92(13)
O2 Cu3 Cu4 85.91(13)	O2 Cu3 O3 167.9(2)	O2 Cu3 O3 91.2(2)
O2 Cu3 O3 91.2(2)	O2 Cu3 O3 167.9(2)	O2 Cu3 O2 91.4(4)
O2 Cu3 O3W 97.13(17)	O2 Cu3 O3W 97.13(17)	O3W Cu3 Cu4 175.62(16)
C9 O4 Cu4 121.5(4)	C23 O11 Cu1 122.5(4)	C1 O6 Cu2 120.2(4)
C8 O1 Cu4 126.0(4)	C11 O9 Cu1 125.2(4)	C22 O7 Cu1 124.4(4)
C9 O3 Cu3 124.2(4)	C23 O12 Cu2 123.3(4)	C8 O2 Cu3 123.5(4)
C22 O8 Cu2 125.8(4)	C11 O10 Cu2 120.8(4)	C1 O5 Cu1 123.5(4)

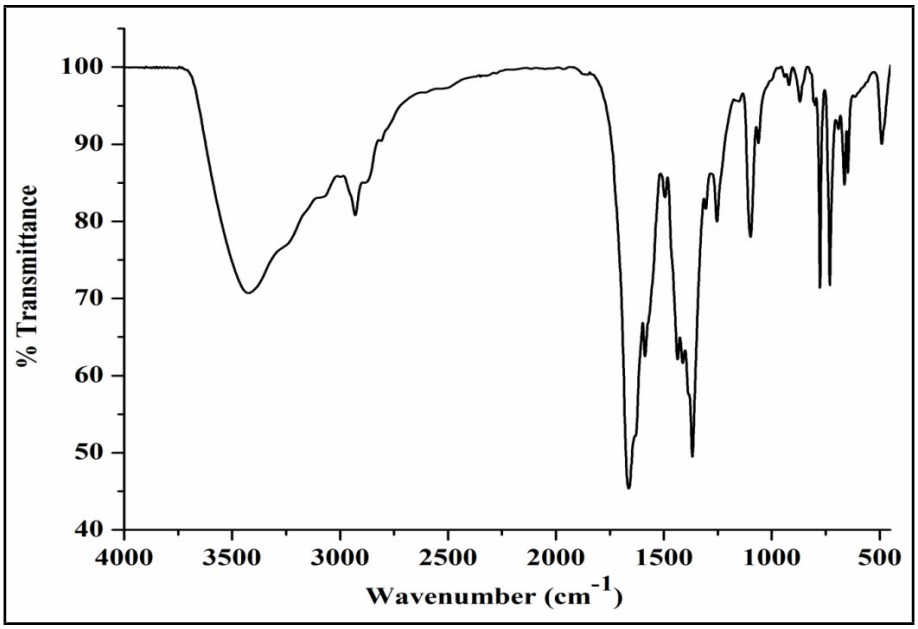

Fig. S9 IR spectrum of **1.**

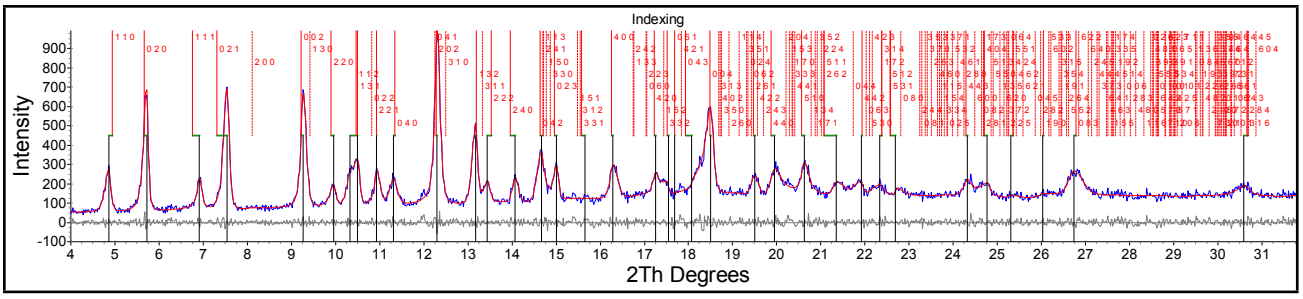

(a)

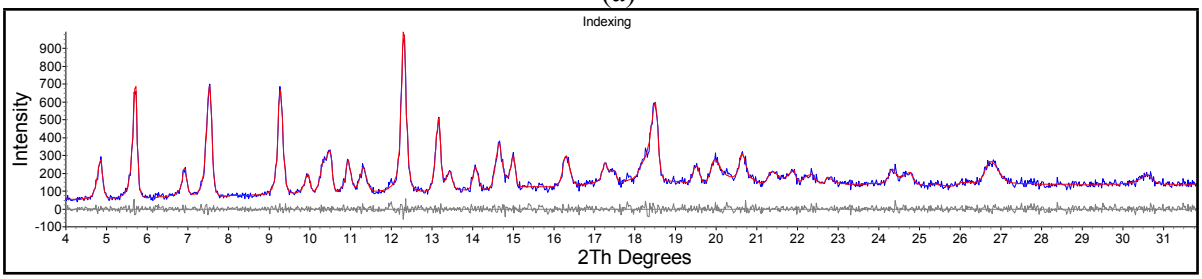

(b)

Fig. S10 (a) observed (blue) and refined (red) X-ray powder diffractograms (the latter obtained from Pawley refinement) as well as the difference plot (grey) for **1** at room temperature with hkl parameters, and (b) Observed (blue) and refined (red) X-ray powder diffractograms (the latter obtained from Pawley refinement) as well as the difference plot (grey) for **1** at room temperature.

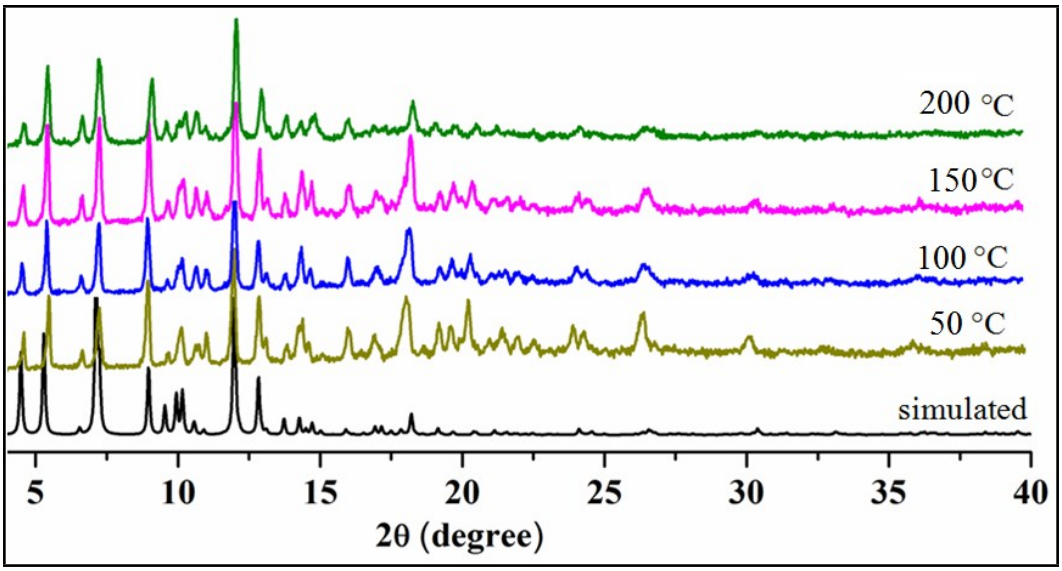

Fig. S11 VTPXRD of compound **1.**

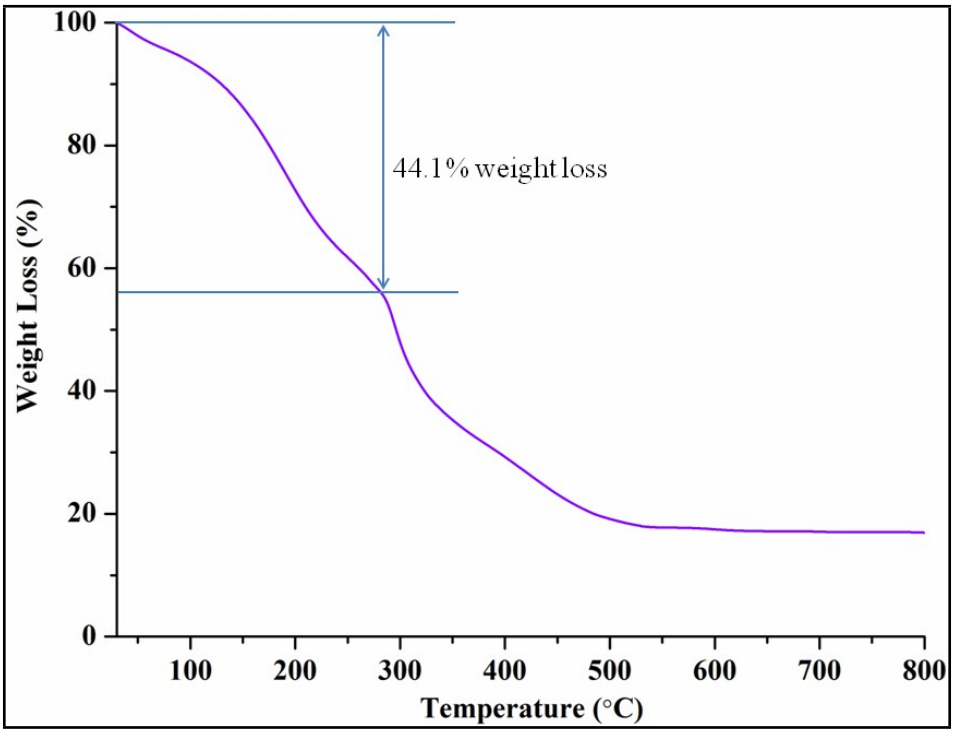

Fig. S12 TGA curve of **1.**

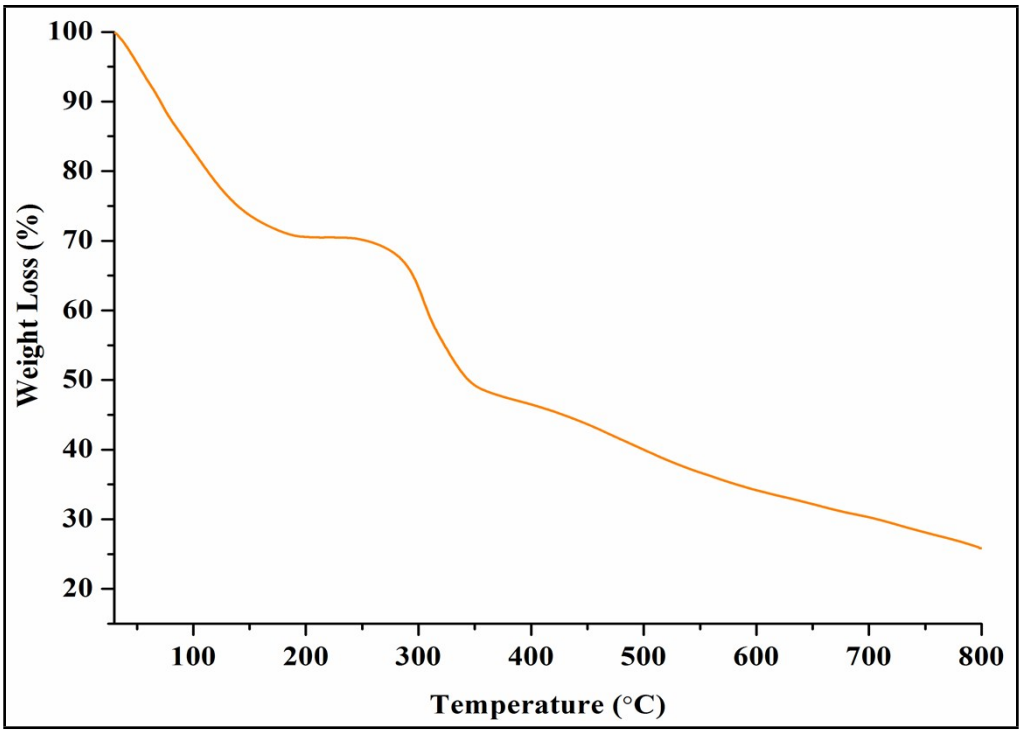

Fig. S13 TGA curve of **1** after acetone exchange.

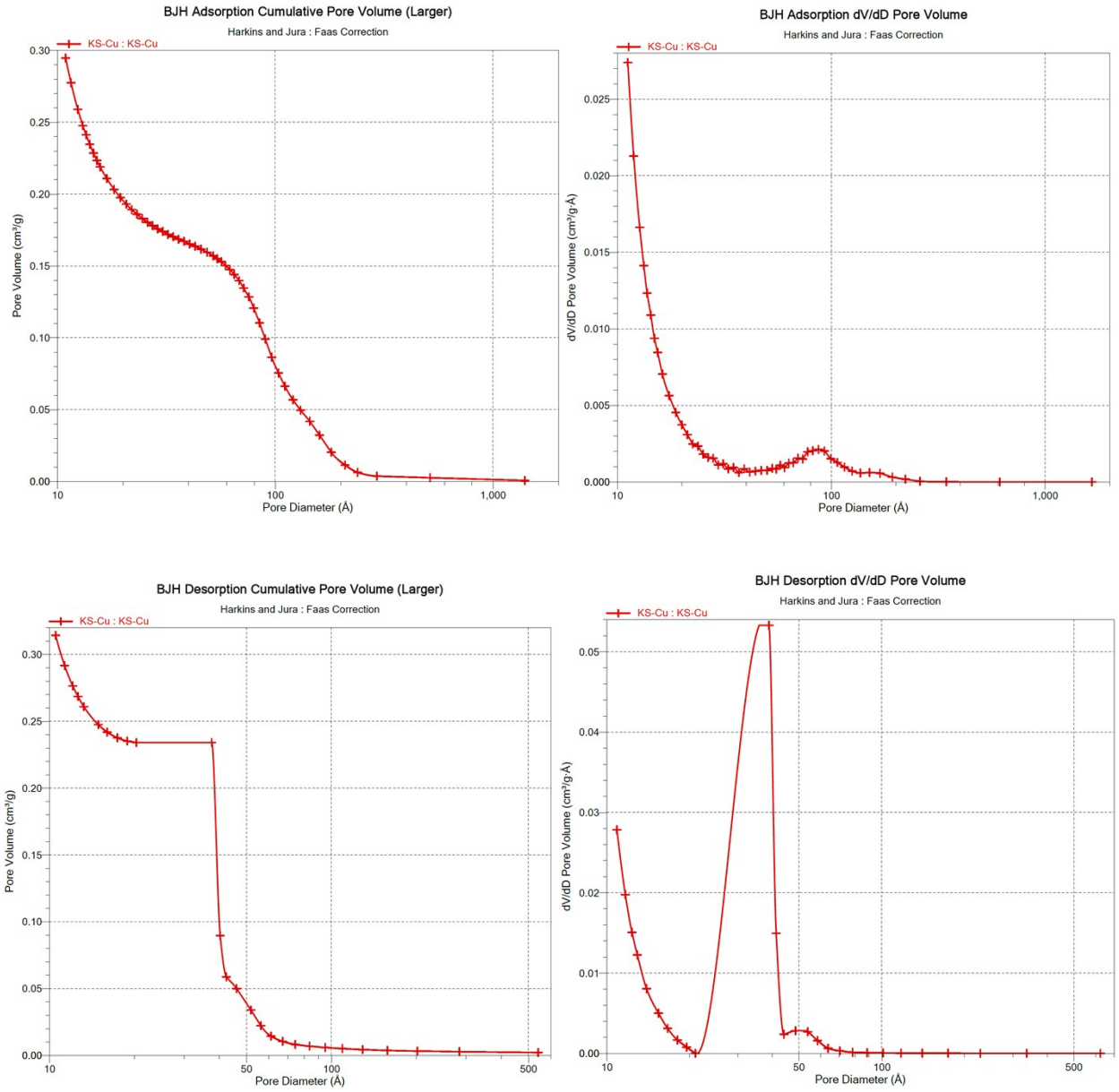

Fig. S14 Pore size distribution in **1′**.

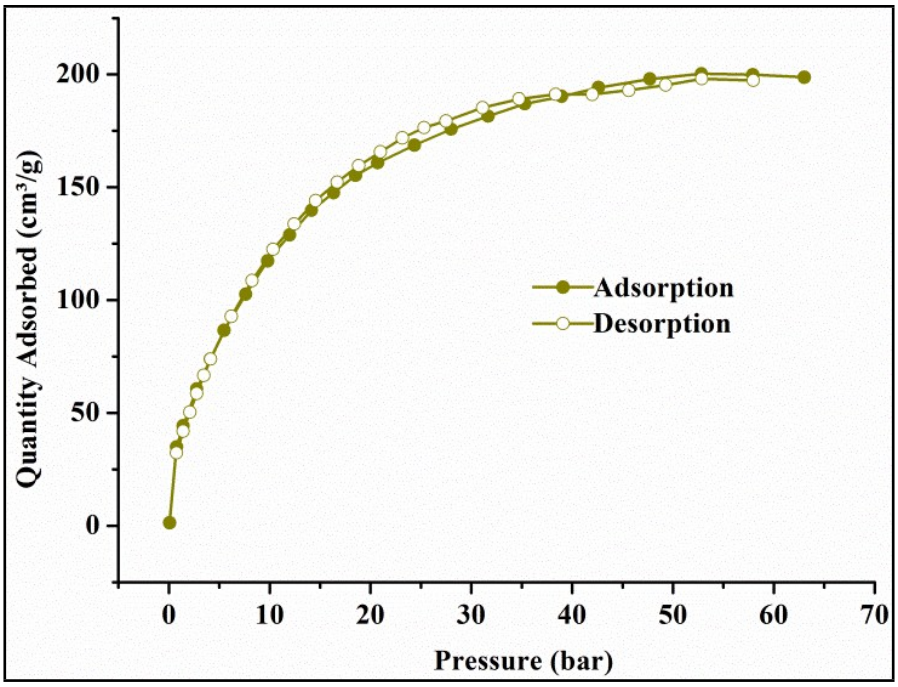

Fig. S15 CH_4 physisorption isotherm for **1′** at 298 K.

Calculation of Isosteric Heat of CO_2 Adsorption (q_{st})

The process to calculate heat of CO_2 adsorption from Clausius-Clapeyron equation is as follows. Two different adsorption isotherms that were measured at different temperatures T_1 (273K) and T_2 (298K) are needed for the analysis. q_{st} at an adsorption amount can be calculated from the equation below with the difference between the two different pressures (p_1 and p_2) at the same adsorption amount.

$$q_{st} = \frac{RT_1T_2}{T_2 - T_1}(\ln p_2 - \ln p_1)$$

Where R is the universal gas constant.

Table S3. Summary of hydrogen uptake of some selected MOFs.

Material	H_2 uptake at 77K and high pressure (wt %)	Volumetric H_2 uptake at 77 K ($g\ L^{-1}$)	Reference
$[Cu_6(L)_3(H_2O)_6]\cdot(14DMF)(9H_2O)$	6.6, 62 bar	49, 62 bar	This Work
UMCM-150, $Cu_3(bhtc)_2$	5.7, 45 bar	36, 45 bar	8
$Be_{12}(OH)_{12}(BTB)_4$	6, 20 bar	44, 100 bar	9
$Cu_2(abtc)$	5.22, 50 bar	40.1, 50 bar	10
DUT-6, $Zn_4O(2,6\text{-ndc})(btb)_{4/3}$	5.64, 50 bar	23.1, 50 bar	11
DUT-9, $Ni_5O_2(btb)_2$	5.85, 40 bar	29.0, 40 bar	12
FJI-1, $Zn_6(BTB)_4(4,4'\text{-bipy})_3$	6.52, 37 bar		13
IRMOF-20, $Zn_4O(ttdc)_2$	6.7, 80 bar	34, 80 bar	14
MIL-101, $Cr_3OF(BDC)_3$	6.1, 80 bar		15
Mn-BTT, $Mn_3[(Mn4Cl)_3(BTT)8]_2$	5.1, 90 bar	43, 90 bar	16
MOF-5, IRMOF-1, $Zn_4O(BDC)_3$	5.75, 35 bar 7.1, 40 bar 10, 100 bar	42.1, 40 bar 66, 100 bar	17 18 18
MOF-177, $Zn_4O(BTB)_2$	7.5, 70 bar	32, 70 bar	19
MOF-200, $Zn_4O(BBC)_2(H_2O)_3\cdot H_2O$	6.9, 80 bar	36, 80 bar	20
MOF-205, $Zn_4O(BTB)_{4/3}(NDC)$	6.5, 80 bar	46, 80 bar	20
MOF-210, $Zn_4O(BTE)_{4/3}(BPDC)$	7.9, 80 bar	44, 80 bar	20
NOTT-101, $Cu_2(tptc)$	(5.71, 20 bar); (6.19, 60 bar)	43.1, 60 bar	21
NOTT-102, $Cu_2(qptc)$	(5.72, 20 bar); (6.72, 60 bar)	42.3, 60 bar	21
NOTT-103, $Cu_2(ndip)$	(6.11, 20 bar); (7.72, 60 bar)	50, 60 bar	21
NOTT-105, $Cu_2(ftptc)$	5.12, 20 bar		21
NOTT-110, $Cu_2(phdip)$	5.43, 55 bar	46.8, 55 bar	22
NU-100, $Cu_3(ttei)$	9.05, 56 bar		23
PCN-10, $Cu_2(aobtc)$	5.23, 45 bar	39.2, 45 bar	24
PCN-11, $Cu_2(sbtc)$	5.04, 45 bar	37.8, 45 bar	24
SNU-5, $Cu_2(abtc)$	5.22, 50 bar	45.8, 50 bar*	10

Table S4. Summary of CO_2 uptake of some selected MOFs.

Chemical Formula	Common Name	Frame work Density (g/cm^3)	P (bar)	T (K)	Capacity			Reference
					cm^3/g	cm^3/cm^3	wt %	
$[Cu_6(L)_3(H_2O)_6]\cdot(14DMF)(9H_2O)$	**1**	0.754	32	298	289.96	218.63	60	This work
$Cr_3O(H_2O)_2F(NTC)_{1.5}$	MIL-102	1.96	30	304	66.18	129.71	13.0	25
$Zn_6O_4(OH)_4(BDC)_6$	UiO-66	1.238	18	303	123.71	153.15	24.3	26
$Cr_3O(H_2O)_2F(BDC)_3$	MIL-101(Cr)	0.62	5.3	283	132.36	82.06	26.0	27
Al(OH)(ndc)	DUT-4	0.773	10	303	134.40	103.89	26.4	28
$Zn_2(BPnDC)_2(bpy)$	SNU-9	1.124	30	298	152.22	171.09	29.9	29
$Cu_3(BTC)_2$	HKUST-1	0.96	300	313	217.89	209.18	42.8	30
$Cr_3O(H2O)_3F(BTC)_2$	MIL-100(Cr)	0.70	50	304	225.02	157.51	44.2	31
Cu_4(TDCPTM)	NOTT-140	0.677	20	293	235.20	159.23	46.2	32
$[Cu(H_2O)]_3$(btei)	PCN-61	0.56	35	298	258.62	144.83	50.8	33
$[Cu(H_2O)]_3$(ntei)	PCN-66	0.45	35	298	272.87	122.79	53.6	33
Ni_2(dobdc)	Ni-MOF-74	1.206	22	278	275.93	332.77	54.2	34
$[Cu_3(H_2O)]_3$(ptei)	PCN-68	0.38	35	298	291.20	110.66	57.2	33
$Zn_4O(BTB)_2$	MOF-177	1.01	50	298	309.53	312.62	60.8	20
$Ni_5O_2(BTB)_2$	DUT-9	0.467	47	298	316.14	147.64	62.1	12
$Zn_4O(BTB)_{4/3}$(NDC)	MOF-205	0.38	50	298	318.69	121.10	62.6	20
$Zn_4O(BDC)_3$	MOF-5, IRMOF-1	0.605	10	273	295.27	178.64	58.0	35
Mg_2(dobdc)	Mg-MOF-74	0.909	36	278	350.76	318.84	68.9	34
Cu_3(TCEPEB)	NU-100	0.273	40	298	355.34	97.01	69.8	36
$Zn_4O(BBC)_2(H_2O)_3$	MOF-200	0.22	50	298	376.22	82.77	73.9	20
$Zn_4O(BTE)_{4/3}$(BPDC)	MOF-210	0.25	50	298	377.75	94.44	74.2	20

Computational Details

We have extracted and simplified the metal organic framework (MOF) structure for the computational study, from the associated experimental crystallographic data of the synthesized MOF. This model for the MOF is necessary in order to reduce the computational cost keeping all relevant interactions intact. We have studied the adsorption of H_2 and CO_2 gas molecules at different positions of the model complex. All of the structures are optimized using density functional theory (DFT) based ωB97x-D[37] functional in conjunction with TZVP basis set. The frequency calculations are performed at ωB97x-D/TZVP level of theory taking the optimized structures. All real frequency values ensure that the optimized structures are at the minima on their respective potential energy surfaces.

Initially two gas molecules (H2 / CO2) were chosen to check the strength and the nature of the interaction with the host. Later on ten more gas molecules were taken to understand whether the interaction energy gets changed drastically and / or the change in the nature of interaction, if any. As our modeled MOF structure has two different types of gas adsorption sites, one is at the vicinity of the Cu-center and another is near the benzene ring, it is expected that the adsorbed gas molecules will interact in two different ways and will exhibit two different types of interaction energies and other related properties (as vindicated by NBO and AIM analyses). First we optimized and characterized the 2Gas@MOF structures. We computed the interaction energy (ΔE_{int}) in between the 2 gas molecules and the MOF and the total interaction energy is decomposed into different energy contributions (ΔE_{pauli}, ΔE_{el}, ΔE_{orb}, ΔE_{disp}). The result shows that the ΔE_{int} is mainly governed by the electrostatic interaction energy (ΔE_{el}). Next we checked the adsorption of 12 gas molecules by MOF (5 benzene rings interact with 10 gas molecules and remaining 2 gas molecules are attached to two different Cu-centers). The 12Gas@MOF

structures were optimized. The calculation of the ΔE_{int} and its decomposition into different energy terms clearly indicate that the adsorption of the gas molecules to the Cu-centers is mainly governed by ΔE_{el} whereas the gas molecules at the vicinity of the benzene rings are bound with dispersion forces (ΔE_{disp}). Thus the calculations with 2Gas@MOF as well as 12Gas@MOF provide meaningful insights into the overall adsorption process vis-à-vis the nature of interaction therein.

For the $12CO_2$@MOF system a couple of imaginary frequencies are obtained but they can be neglected because of their very small values. The charge (q) on each atomic centre is obtained by natural population analysis (NPA)[38] and the bond order between two atoms is obtained from the Wiberg bond index (WBI)[39] calculations using the natural bond orbital (NBO) scheme.[40] All these computations are done by using a fine grid, with 75 radial shells per atom, and 302 angular points per shell using the Gaussian 09 suite of program package.[41]

The energy decomposition analysis (EDA)[42] is performed at rev-PBE-D3/TZ2P//ωB97x-D/TZVP level of theory using ADF 2013.01 program.[43,44] The EDA decomposes the interaction energy (ΔE_{int}) into four energy terms, *viz*., the Pauli repulsion (ΔE_{pauli}), the electrostatic interaction energy (ΔE_{el}), the orbital interaction energy (ΔE_{orb}), and the dispersion interaction energy (ΔE_{disp}) as,

$$\Delta E_{int} = \Delta E_{pauli} + \Delta E_{el} + \Delta E_{orb} + \Delta E_{disp} \qquad (1)$$

The ΔE_{pauli} represents the repulsion between the electrons in the occupied orbitals of the interacting fragments. The ΔE_{el} term presents the quasi-classical electrostatic interaction energy between the fragments under consideration. In general the ΔE_{el} term is attractive in nature. The next attractive contribution in energy comes from the orbital interaction energy, ΔE_{orb}, which arises due to the charge transfer and mixing of the occupied and unoccupied orbitals between the

fragments and polarization effect. The ΔE_{disp} represents the dispersion energy correction towards the total attraction energy.

The topological analysis of the electron density[45] is carried out at the ωB97x-D/TZVP level of theory. Several density based parameters are computed to find out the nature of the interactions. These calculations are performed using Multiwfn software package.[46]

Identification of the non-covalent interaction between the guest gas molecules and host MOF is carried out using the NCIPLOT software.[47,48] The NCI analysis is based on the electron density (ρ) and its reduced density gradient (s), as,

$$s = \frac{1}{2(3\pi^2)^{1/3}} \frac{|\nabla\rho|}{\rho^{4/3}} \qquad (2)$$

where, $\nabla\rho$ is the gradient of ρ.

The low ρ and low s values signify a weak, non-covalent interaction in between the molecular pairs. The Laplacian of electron density ($\nabla^2\rho$) is a parameter for describing the nature of the interaction in between the molecular pairs. But, different types of non-covalent interactions (steric interactions, hydrogen bonds, van der Waals' (vdW) interactions) cannot be distinguished by $\nabla^2\rho$ index itself. The eigenvalues λ_i of electron density Hessian (second derivative) matrix such that $\nabla^2\rho = \lambda_1 + \lambda_2 + \lambda_3$ ($\lambda_1 < \lambda_2 < \lambda_3$), is useful in the identification of the non-covalent interactions. The sign of the λ_2 varies with the nature of the interaction. As for H-bonds, $\lambda_2 < 0$, for steric interactions, $\lambda_2 > 0$ and for vdW type of interaction $\lambda_2 \lesssim 0$. Thus, s is plotted against sign(λ_2)ρ (product of sign(λ_2) and ρ). The positions of the troughs associated with the $s(\rho)$

appearing in the 2D plot give an idea about the type of the non-covalent interaction. The real space intermolecular interaction iso-surface is generated using VMD visualization package.[49]

Table S5. The structural parameters of nH_2@MOF computed at the ωB97x-D/TZVP level of theory.

	r(Cu-H_2)	r(H-H)	r(RC-H_2) †
Free H_2		0.744	
$2H_2$@MOF	2.245; 2.250	0.750, 0.750	
$12H_2$@MOF	2.301; 2.299	0.750; 0.750; 0.745; 0.745; 0.745; 0.745; 0.745; 0.745; 0.745; 0.745; 0.745; 0.746	2.676; 2.701; 2.704; 2.702; 2.700; 2.703; 2.697; 2.718; 2.678; 2.695

All units are in Å; † RC = Ring Centre

Table S6. The structural parameters of nCO_2@MOF computed at the ωB97x-D/TZVP level of theory.

	r(Cu-O)	r(C-O1/O2) †	∠O1-C-O2
Free CO_2		1.156	180.0
$2CO_2$@MOF	2.523, 2.503	1.160, 1.152; 1.161, 1.151	178.1; 178.3
$12CO_2$@MOF	2.419, 2.423	1.161, 1.152; 1.161, 1.151; 1.155, 1.157; 1.157, 1.156; 1.157, 1.155; 1.157, 1.156; 1.155, 1.157; 1.156, 1.156; 1.160, 1.154; 1.156, 1.155; 1.160, 1.153; 1.155, 1.157	178.2; 178.4; 178.7; 177.8; 179.3; 179.2; 179.3; 179.4; 178.6; 178.8; 178.9; 179.2

All bond lengths (r) are in Å and angles are in º; † O1 is the closest O atom of CO_2 near the Cu-atom in nCO2@MOF.

Table S7. The energy decomposition analysis (EDA) results at the rev-PBE-D3/TZ2P//wB97x-D/TZVP level.

nGas@MOF	Fragments	ΔE_{pauli}	ΔE_{el}	ΔE_{orb}	ΔE_{disp}	ΔE_{int}	ΔE_{int}/Gas
$2H_2$@MOF	$2H_2$ + MOF	21.5	-13.3 (47.5)	-9.3 (33.2)	-5.4 (19.3)	-6.4	-3.2
$12H_2$@MOF	$12H_2$ + MOF	41.8	-19.7 (31.5)	-16.2 (25.9)	-26.6 (42.6)	-20.7	-1.7
	$10H_2$+$2H_2$@MOF	20.6	-6.6 (17.6)	-9.8 (25.9)	-21.3 (56.4)	-17.1	-1.7
$2CO_2$@MOF	$2CO_2$ + MOF	32.7	-22.5 (50.5)	-11.2 (25.2)	-10.8 (24.2)	-11.9	-6.0
$12CO_2$@MOF	$12CO_2$ + MOF	82.1	-45.9 (35.7)	-23.6 (18.3)	-59.3 (46.0)	-46.8	-3.9
	$10CO_2$+$2CO_2$@MOF	44.0	-20.4 (23.9)	-14.0 (16.4)	-50.9 (59.7)	-41.3	-4.1

Table S8. Different electron density descriptors computed at ωB97x-D/TZVP level.

BCP points	**Type**	**$\rho(r_c)$**	**$\nabla^2\rho(r_c)$**	**$G(r_c)$**	**$K(r_c)$**	**$V(r_c)$**	**$H(r_c)$**	**ELF**
$2H_2$@MOF								
H-H	(3,-1)	0.25949	-0.26505	-1.05864	0.00038	0.26505	-0.26543	1.00000
Cu-H	(3,-1)	0.02197	0.00070	0.07469	0.01797	-0.00070	-0.01727	0.07039
$12H_2$@MOF								
H-H(@Cu	(3,-1)	0.25946	-0.26500	-1.05849	0.00037	0.26500	-0.26537	1.00000
Cu-H	(3,-1)	0.02172	0.00070	0.07352	0.01768	-0.00070	-0.01699	0.06999
C-H	(3,-1)	0.00438	0.00075	0.01511	0.00303	-0.00075	-0.00228	0.01212
H-H(@Ar	(3,-1)	0.26160	-0.26812	-1.07187	0.00015	0.26812	-0.26826	1.00000
H_2-H_2	(3,-1)	0.00197	0.00045	0.00688	0.00127	-0.00045	-0.00082	0.00479
$2CO_2$@MOF								
Cu-O	(3,-1)	0.02221	0.10275	0.02403	-0.00165	-0.02238	0.00165	0.04205
O(in CO_2)-H(aromatic ring)	(3,-1)	0.00328	0.01318	0.00246	-0.00083	-0.00162	0.00083	0.00705
O-C (of CO_2)	(3,-1)	0.46778	0.37420	0.93778	0.84423	-1.78201	-0.84423	0.42688
$12CO_2$@MOF								
Cu-O	(3,-1)	0.02619	0.12765	0.03043	-0.00148	-0.02895	0.00148	0.04533
O(in CO_2)-H(aromatic ring)	(3,-1)	0.00588	0.02305	0.00449	-0.00128	-0.00321	0.00128	0.01475
C(in CO_2)-C(aromatic ring)	(3,-1)	0.00526	0.01823	0.00364	-0.00092	-0.00271	0.00092	0.01550
O(in CO_2)-C(aromatic ring)	(3,-1)	0.00089	0.00337	0.00058	-0.00026	-0.00032	0.00026	0.00157
O-O (of two different CO_2)	(3,-1)	0.00500	0.02318	0.00425	-0.00155	-0.00270	0.00155	0.00964
O-C (of two different CO_2)	(3,-1)	0.00534	0.02477	0.00474	-0.00145	-0.00329	0.00145	0.00961
O-C (of same CO_2)	(3,-1)	0.45792	0.23905	0.88054	0.82077	-1.70131	-0.82077	0.44039

Table S9. The NBO analysis of nH_2@MOF at wB97x-D/TZVP level.

	qH_2 (qH,qH)	q(Cu)	WBI(H-H)	WBI(Cu-H)
Free H_2	0.000 (0.000, 0.000)		1.0000	
$2H_2$@MOF	0.043 (0.021, 0.022);	1.037;	0.9522;	(0.0450, 0.0454);
	0.045 (0.020,0.025)	1.036	0.9517	(0.0448,0.0446)
$12H_2$@MOF	0.057 (0.028, 0.029);	0.425;	0.9524;	(0.0448, 0.0447);
	0.057 (0.025, 0.032);	0.426	0.9521;	(0.0447,0.0445)
	-0.006 (0.012, -0.018);		0.9983;	
	-0.004 (0.014, -0.018);		0.9982;	
	-0.005 (0.013, -0.018);		0.9982;	
	-0.006 (0.011, -0.017);		0.9982;	
	-0.005 (0.012, -0.017);		0.9982;	
	-0.006 (0.012, -0.018);		0.9982;	
	-0.002 (0.015, -0.017);		0.9980;	
	-0.001 (0.012, -0.013);		0.9979;	
	-0.004 (0.009, -0.013);		0.9980;	
	-0.002 (0.007, -0.009);		0.9976	

Table S10. The NBO analysis of nCO_2@MOF at wB97x-D/TZVP level.

	qCO_2 (qO1, qC, qO2)	q(Cu)	WBI(C-O1), WBI(C-O2)	WBI(Cu-O1)
Free CO_2	0.000 (-0.483, 0.967, -0.483)		1.9108,1.9111	
$2CO_2$@MOF	0.035 (-0.509, 1.018, -0.474)	1.062	1.8488, 1.9358;	0.0623
	0.036 (-0.514, 1.013, -0.463)	1.059	1.8387, 1.9490	0.0658
$12CO_2$@MOF	0.044 (-0.508, 1.019, -0.467)	1.060	1.8373, 1.9443;	0.0821
	0.045 (-0.509, 1.021, -0.467)	1.062	1.8381, 1.9445;	0.0827
	-0.001 (-0.498, 0.984, -0.487)		1.8985, 1.9117;	
	-0.001 (-0. 498, 0.984, -0.487)		1.8973, 1.9117;	
	-0.001 (-0. 498, 0.985, -0.488)		1.8987, 1.9112;	
	0.000 (-0. 489, 1.003, -0.514)		1.8832, 1.9130;	
	0.001 (-0.474, 0.990, -0. 515)		1.8951, 1.9123;	
	0.001 (-0.496, 0.994, -0.497)		1.8945, 1.9109;	
	0.000 (-0.500, 0.988, -0.488)		1.8793, 1.9256;	
	-0.001 (-0.477, 0.990, -0. 514)		1.8778, 1.9285;	
	0.001 (-0.502, 0.991, -0.488)		1.9022, 1.9015;	
	-0.001 (-0.501, 0.987, -0.487)		1.8946, 1.9121	

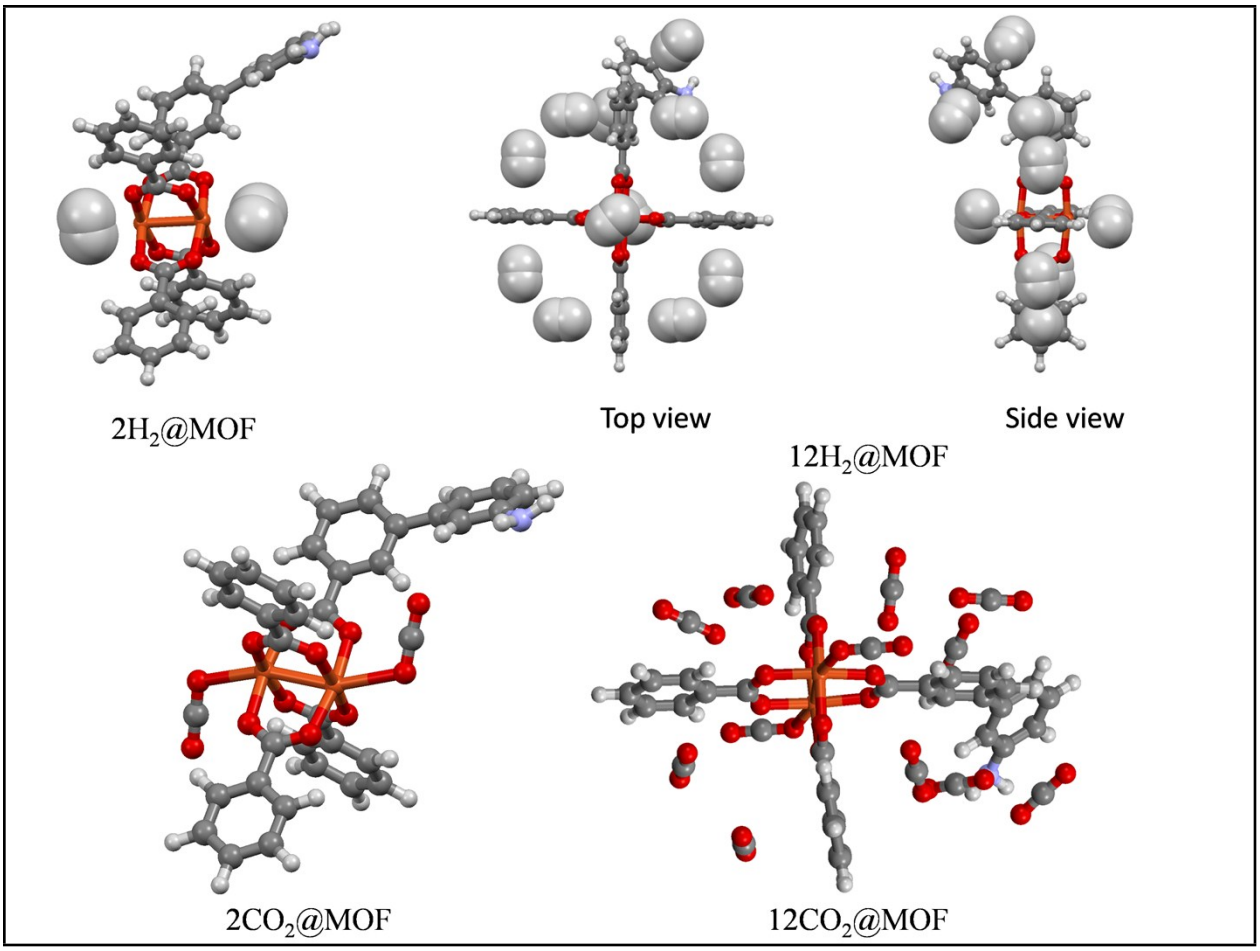

Fig. S16 The optimized geometries of the gas adsorbed MOF systems obtained at the wB97x-D/TZVP level of theory.

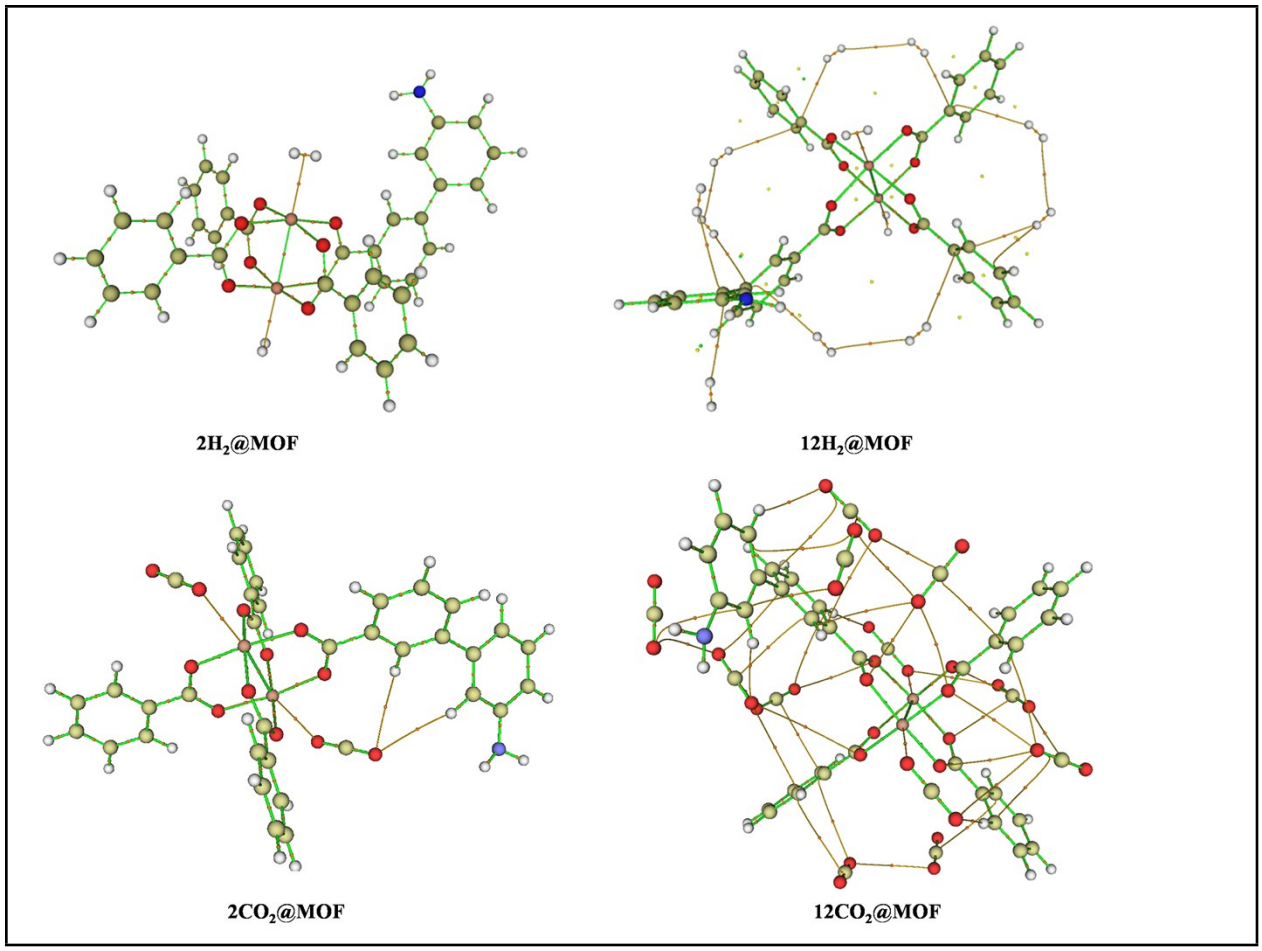

Fig. S17 Different critical points of the gas adsorbed MOF systems obtained at the ωB97x-D/TZVP level of theory.

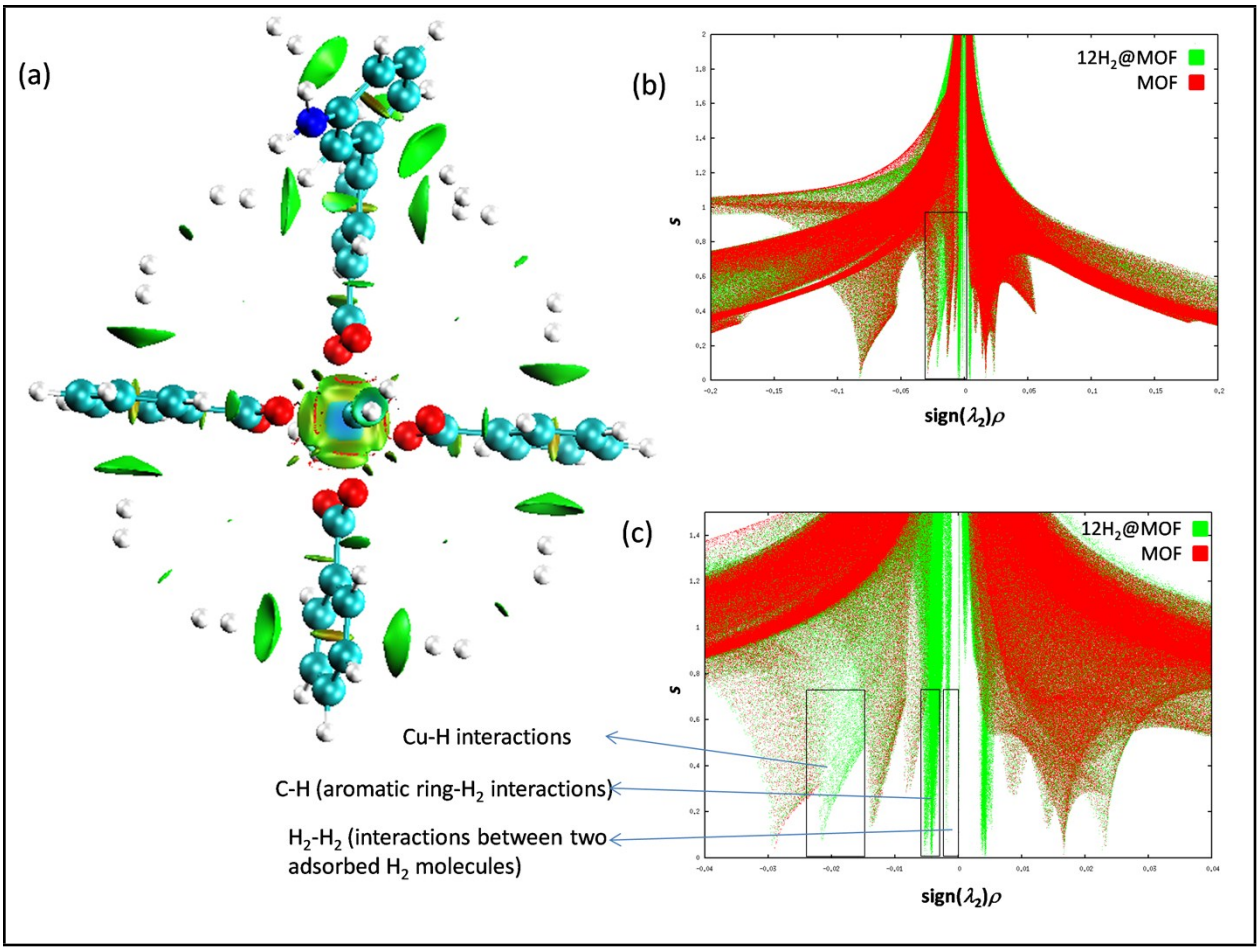

Fig. S18 (a) NCI isosurface plot of $12H_2$@MOF. The isosurface is generated for s = 0.5 a.u., (b) The plot of reduced gradient versus sign(λ_2)ρ of the $12H_2$@MOF system, (c) zoomed view of the plot of reduced gradient versus sign(λ_2)ρ of the $12H_2$@MOF system.

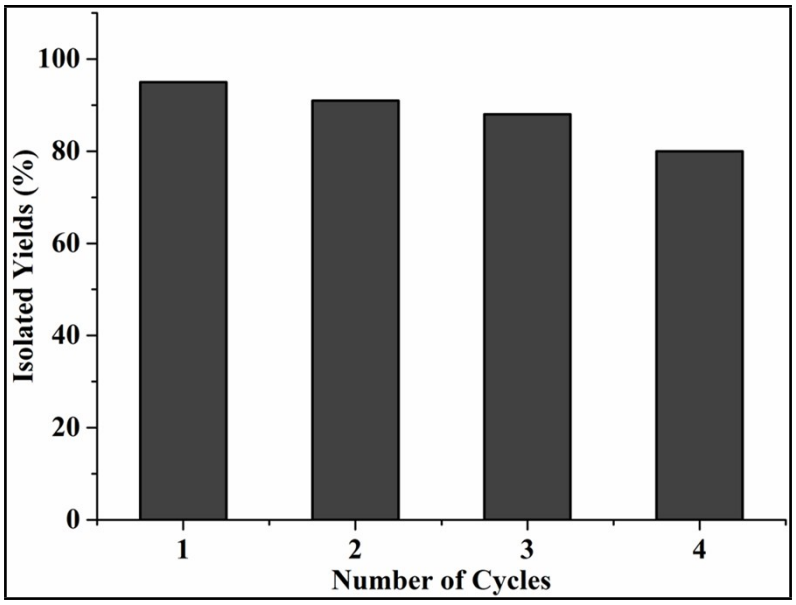

Fig. S19 Recyclability study (four cycles) for catalytic activities of **1** in coupling reactions of epoxides and CO_2.

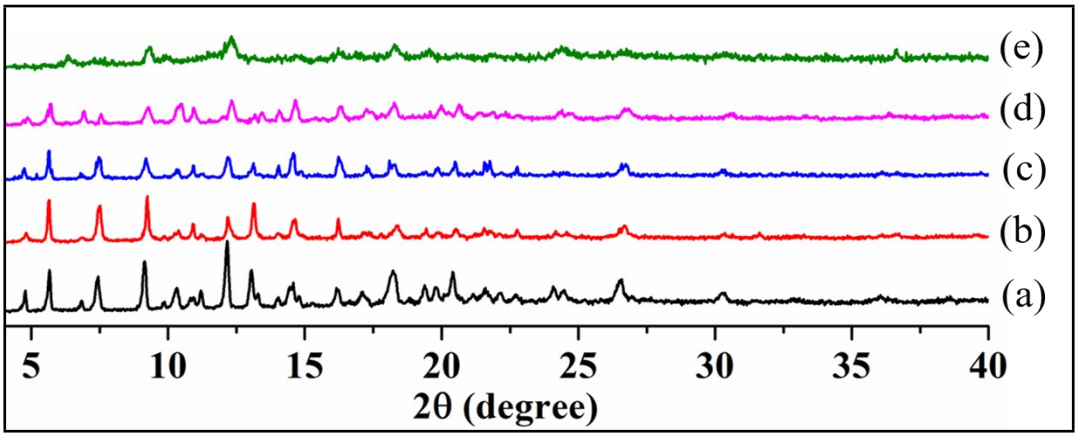

Fig. S20 PXRD patterns of **1** after different catalytic cycle in coupling reactions of epoxides and CO_2.: (a) before catalysis, and after (b) 1st catalytic cycle, (c) 2nd catalytic cycle, (iv) 3rd catalytic cycle and (v) 4th catalytic cycle.

NMR of Catalysis Experiments

Coupling Reactions of Epoxides and CO_2

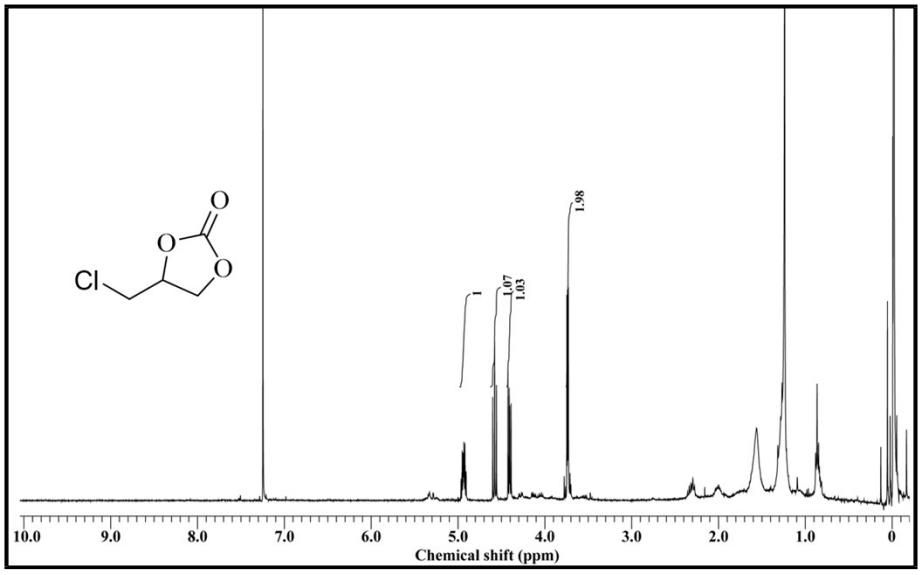

Fig. S21 ^{1}H NMR spectrum of 4-(chloromethyl)-1,3-dioxolan-2-one in $CDCl_3$.

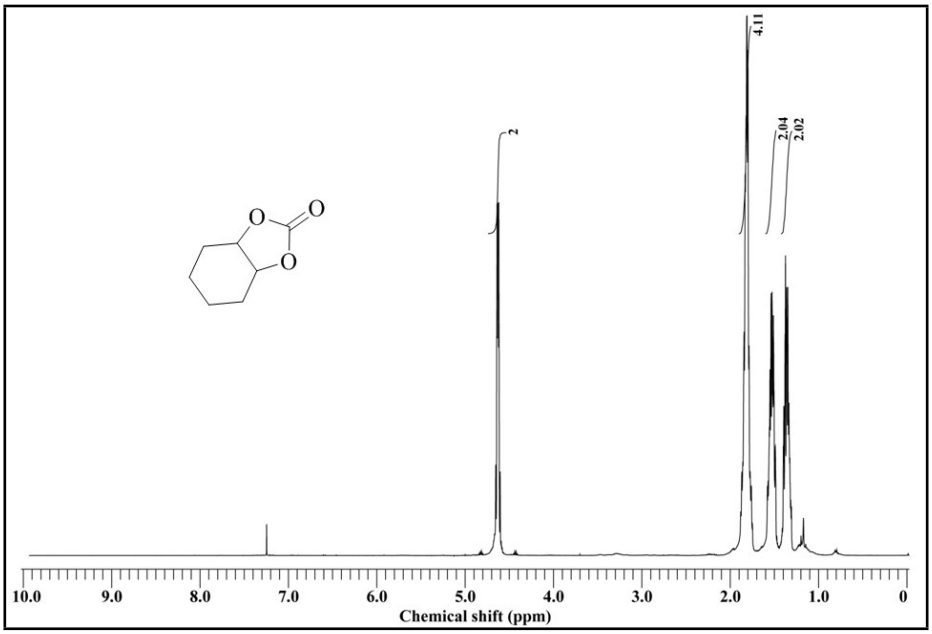

Fig. S22 ^{1}H NMR spectrum of hexahydrobenzo[d][1,3]dioxol-2-one in $CDCl_3$.

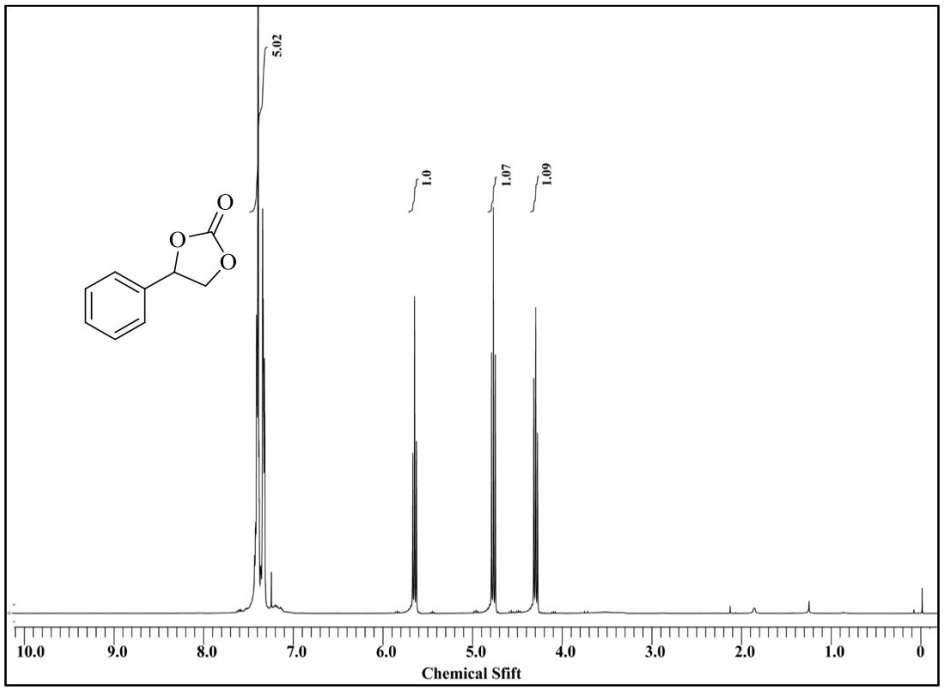

Fig. S23 ^{1}H NMR spectrum of 4-phenyl-1,3-dioxolan-2-one in $CDCl_3$.

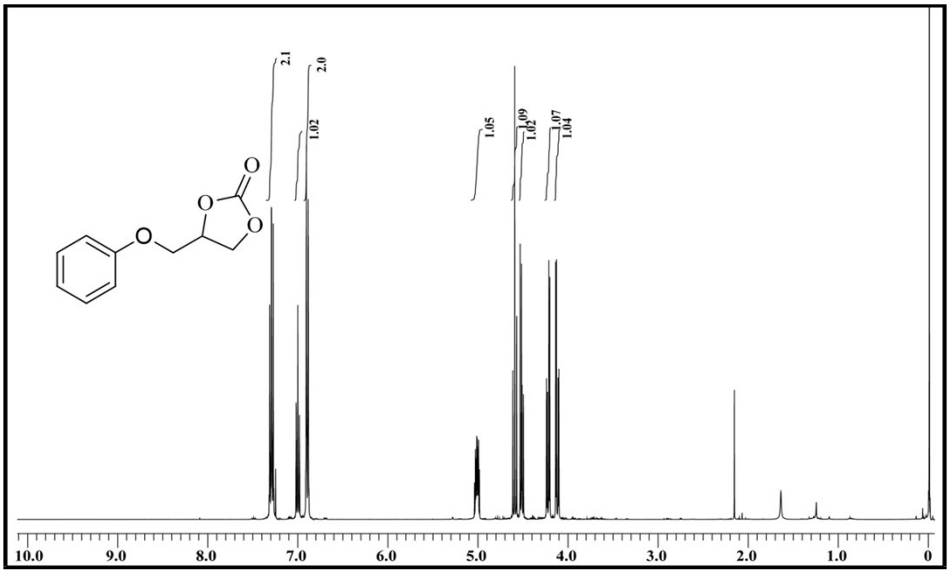

Fig. S24 ^{1}H NMR spectrum of 4-(phenoxymethyl)-1,3-dioxolan-2-one in $CDCl_3$.

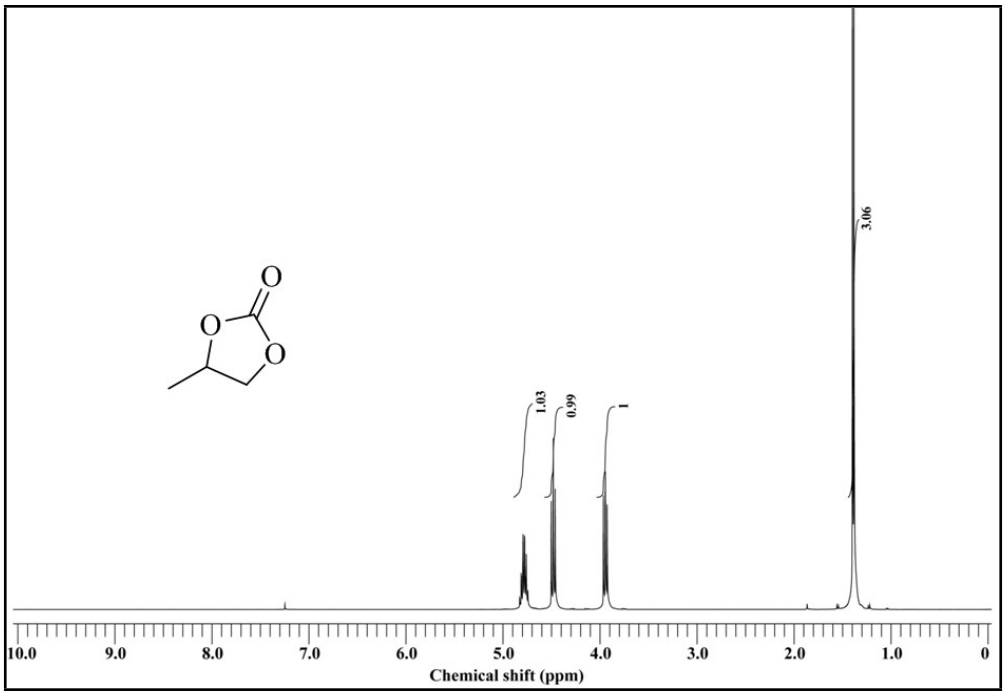

Fig. S25 ^{1}H NMR spectrum of 4-methyl-1,3-dioxolan-2-one in $CDCl_3$.

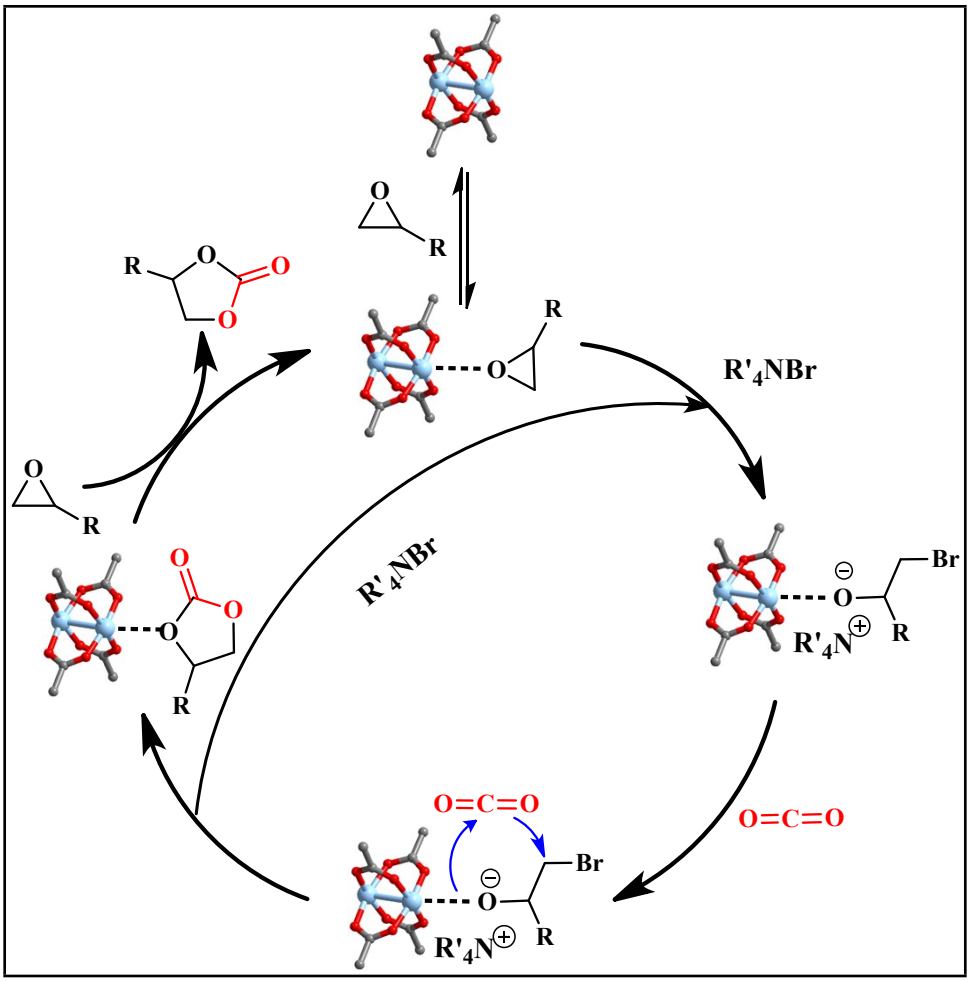

Scheme S2. Proposed mechanism for the **1′** catalyzed carbon dioxide fixation into epoxide in the presence of TBAB.

REFERENCES

1 (*a*) D. De, T. K. Pal, S. Neogi, S. Senthilkumar, D. Das, S. S. Gupta and P. K. Bharadwaj, *Chem. Eur. J.*, 2016, **22**, 3387–3396; (*b*) S. H. Chanteau and J. M. Tour,. *J. Org. Chem.*, 2003, **68**, 8750–8766.

2 *SMART* & *SAINT* Software Reference manuals, Version 6.45; Bruker Analytical X-ray

Systems, Inc.: Madison, WI, **2003**.

3 G. M. Sheldrick, *SADABS*, a software for empirical absorption correction, Ver. 2.05; University of Göttingen: Göttingen, Germany, **2002**.

4 (*a*) *SHELXTL* Reference Manual, Ver. 6.1; Bruker Analytical X-ray Systems, Inc.: Madison, WI, **2000**; (*b*) G. M. Sheldrick, *SHELXTL*, Ver. 6.12; Bruker AXS Inc.: WI. Madison, **2001**.

5 G. M. Sheldrick, *Acta Crystallogr. Sect. A: Fundam. Crystallogr*., 2008, **64**, 112–122.

6 O. V. Dolomanov, L. J. Bourhis, R. J. Gildea, J. A. K. Howard and H. Puschmann, *J. Appl. Crystallogr.*, 2009, **42**, 339–341.

7 A. L. Spek, *J. Appl. Cryst*., 2003, **36**, 7–13.

8 A. G. Wong-Foy, O. Lebel and A. J. Matzger, *J. Am. Chem. Soc*., 2007, **129**, 15740–15741.

9 K. Sumida, M. R. Hill, S. Horike, A. Dailly and J. R. Long, *J. Am. Chem. Soc*., 2009, **131**, 15120–15121.

10 Y.-G. Lee, H. R. Moon, Y. E. Cheon and M. P. Suh, *Angew. Chem. Int. Ed*., 2008, **47**, 7741–7745.

11 N. Klein, I. Senkovska, K. Gedrich, U. Stoeck, A. Henschel, U. Mueller and S. Kaskel., *Angew. Chem. Int. Ed.*, 2009, **48**, 9954–9957.

12 K. Gedrich, I. Senkovska, N. Klein, U. Stoeck, A. Henschel, M. R. Lohe, I. A. Baburin, U. Mueller and S. Kaskel, *Angew. Chem. Int. Ed*., 2010, **49**, 8489–8492.

13 D. Han, F. -Jiang, M.-Y.Wu, L. Chen, Q.-H. Chen and M.-C. Hong, *Chem. Commun*., 2011, **47***,* 9861–9863.

14 A. G. Wong-Foy, A. J. Matzger and O. M. Yaghi, *J. Am. Chem. Soc*., 2006, **128**, 3494–3495.

15 M. Latroche, S. Surblé, C. Serre, C. Mellot-Draznieks, P. L. Llewellyn, J.-H. Lee, J.-S. Chang, S. H. Jhung and G. Férey, *Angew. Chem. Int. Ed.*, 2006, **45**, 8227–8231.

16 M. Dinca, A. Dailly, Y. Liu, C. M. Brown, D. A. Neumann and J. R. Long, *J. Am. Chem. Soc*., 2006**, 128**, 16876–16883.

17 W. Zhou, H. Wu, M. R. Hartman and T. Yildirim, *J. Phys. Chem. C.,* 2007, **111**, 16131–16137.

18 S. S. Kaye, A. Dailly, O. M. Yaghi and J. R. Long, *J. Am. Chem. Soc*., 2007, **129**, 14176–14177.

19 J. L. C. Rowsell and O. M. Yaghi, *J. Am. Chem. Soc.*, 2006, **128**, 1304–1315.

20 H. Furukawa, N. Ko, Y. B. Go, N. Aratani, S. B. Choi, E. Choi, A. Ö. Yazaydin, R. Q. Snurr, M. O'Keeffe, J. Kim and O. M. Yaghi, *Science*, 2010, **329***,* 424–428.

21 X. Lin, I. Telepeni, A. J. Blake, A. Dailly, C. M. Brown, J. M. Simmons, M. Zoppi, G. S. Walker, K. M. Thomas, T. J. Mays, P. Hubberstey, N. R. Champness and M. Schröder, *J. Am. Chem. Soc*., 2009, **131**, 2159–2171.

22 S. Yang, X. Lin, A. Dailly, A. J. Blake, P. Hubberstey, N.R. Champness and M. Schröder, *Chem. Eur. J*., 2009, **15***,* 4829–4835.

23 O. K. Farha, A.Ö. Yazaydin, I. Eryazici, C. D. Malliakas, B. G. Hauser, M. G. Kanatzidis, S. T. Nguyen, R. Q. Snurr and J. T. Hupp, *Nat. Chem*., 2010, **2***,* 944–948.

24 X-. S. Wang, M. Shengqian, K. Rauch, J. M. Simmons, D. Yuan, X. Wang, T. Yildirim, W. C. Cole, J. J. López, A. de. Meijere and H.-C. Zhou, *Chem. Mater*., 2008, **20**, 3145–3152.

25 S. Surblé, F. Millange, C. Serre, T. Duren, M. Latroche, S. Bourrelly, P. L. Llewellyn and G. Férey, *J. Am. Chem. Soc*., 2006, **128**, 14889-14896.

26 A. D. Weirsum, E. S. Lenoir, Q. Yang, B. Moulin, V. Guillerm, M. B. Yahia, S. Bourrelly,; Vimont, A.; Miller, S.; Vagner, C.; M. Daturi, C. Guillaume,. C. Serre,. G. Maurin, P. L. Llewellyn, *Chem. Asian J*., 2011, **6**, 3270–3280.

27 P. Chowdhury, C. Bikkina and S. Gumma, *J. Phys. Chem. C.*, 2009, **113**, 6616–6621.

28 I. Senkovska,. F. Hoffmann, M. Fröba, J. Getzschmann, W. Böhlmann and S. Kaskel, *Microporous Mesoporous Materials,* 2009, **122**, 93–98.

29 H. J. Park and M. P. Suh, *Chem. Commun*., 2010, **46**, 610–612.

30 J. Moellmer, A. Moeller, F. Driesbach, R. Glaeser and R. Staudt, *Microporous Mesoporous Materials,* 2011, **138**, 140–148.

31 P. L. Llewellyn, S. Bourrelly, C. Serre, A.Vimont, M. Daturi, L. Hamon, G. D. Weireld, J.-S. Chang, D.-Y. Hong, Y. K. Hwang, S. H. Jhung and G. Férey, *Langmuir,* 2008, **24**, 7245–7250.

32 C. Tan, S. Yang, N. R. Champness, X. Lin, A. J. Blake, W. Lewis and M. Schröder, *Chem. Commun*., 2011, **47**, 4487–4489.

33 D. Yuan, D. Zhao, D. Sun and H.-C. Zhou, *Angew. Chem. Int. Ed*., 2010, **49**, 5357–5361.

34 P. D. C. Dietzel, V. Besikiotis and R. Blom, *J. Mater. Chem*., 2009, **19**, 7362–7370.

35 J. A. Botas, G. Calleja, M. Sanchez-Sanchez and M. G. Orcajo,. *Langmuir*, 2010, **26**, 5300–5303.

36 O. K. Farha, A.Ö. Yazaydin, I. Eryazici, C. D. Malliakas, B. G. Hauser, M. G. Kanatzidis, S. T. Nguyen, R. Q. Snurr and J. T. Hupp, *Nat. Chem*., 2010, **2***,* 944–948.

37 J.-D. Chai, and M. Head-Gordon, *Phys. Chem. Chem. Phys.,* 2008, **10**, 6615–6620.

38 A. E. Reed, R. B. Weinstock and F. Weinhold, *J. Chem. Phys.,* 1985, **83**, 735–746.

39 K. B. Wiberg, *Tetrahedron*., 1968, **24**, 1083–1096.

40 A. E. Reed, L. A. Curtiss and F. Weinhold, *Chem. Rev.,* 1988, **88**, 899–926.

41 M. J. Frisch, *et al.* Gaussian 09, Revision C.01, Gaussian, Inc., Wallingford CT, 2009.

42 M. P. Mitoraj, A. Michalak and T. A. Ziegler, *J. Chem. Theory Comput.*, 2009, **5**, 962–975.

43 E. J. Baerends, *et al. ADF2013.01*, SCM, *Theoretical Chemistry*, Vrije Universiteit, Amsterdam, The Netherlands, 2013.

44 G. te Velde, F. M. Bickelhaupt, E. J. Baerends, C. F. Guerra, S. J. A. Van Gisbergen, J. G. Snijders and T. Ziegler, *J. Comput. Chem.*, 2001, **22**, 931–967.

45 R. F. W. Bader, *Atoms in Molecules: A Quantum Theory*, Oxford University Press: Oxford, UK, 1990.

46 T. Lu and F. W. Chen, *J. Comput. Chem*., 2012, **33***,* 580–592.

47 E. R. Johnson, S. Keinan, P. Mori-Sanchez, J. Contreras-Garcia, A. J. Cohen and W. Yang, *J. Am. Chem. Soc.,* 2010, **132**, 6498–6506.

48 J. Contreras-Garcia, E. R. Johnson, S. Keinan, R. Chaudret, J.-P. Piquemal, D. N. Beratan and W. Yang, *J. Chem. Theory Comput.,* 2011, **7**, 625–632.

49 W. Humphrey, A. Dalke and K. Schulten, *J. Molec. Graphics,* 1996, **14**, 33–38.